Supplementary Information

Ultra-high surface area ionic-liquid-derived carbons that meet both gravimetric and volumetric methane storage targets

Nawaf Albeladi, L. Scott Blankenship and Robert Mokaya*

School of Chemistry, University of Nottingham, University Park, Nottingham NG7 2RD, U. K.

E-mail: r.mokaya@nottingham.ac.uk (R. Mokaya)

Using the whittaker method in pyGAPS

First install pyGAPS – see instructions at https://pygaps.readthedocs.io/en/master/installation.html

Currently the whittaker module is not implemented in the graphical interface, so the following instructions require some knowledge of python.

1. Import required modules;

```
import pygaps.parsing as pgp
import pygaps.characterisation as pgc
```

2. Parse the isotherm, for example

```
isotherm = pgp.isotherm_from_aif('/path/to/file')
```

Or from a manufacturer-specific file e.g. from a micromeritics .xlsx file;

```
Isotherm = pgp.isotherm_from_commercial(
     `path/to/file`,
     'mic', 'xl',
     )
```

This can be used as-is, but if desired, the isotherm can first be modeled to check goodness of fit;

```
import pygaps.modelling as pgm

# additional parameters can be adjusted
model = pgm.model_iso(isotherm, model='Toth')
```

3. Calculate whittaker enthalpy. The model and loadings at which to calculate can be specified.

```
whittaker = pgc.enthalpy_sorption_whittaker(
     isotherm, # or use model
     model='Toth', # ignored for modeled isotherms
     loading=isotherm.loading(), # use original loadings
     verbose=True, # plots the isotherm for you
)

# data can then be exported, e.g.
whittaker.to_csv('path/to/save.csv')
```

Supplementary Table 1 Parameters for the determination of BETSI surface area for IL-ACxT carbons.

Sample	BETSI surface area (m^2 g^{-1})	Points	r^2	Slope	Intercept	C	Qm (cm^3 g^{-1} STP)
IL-AC2700	1783	10	0.9998	0.002436	5.005×10^{-6}	488	410
IL-AC2800	2519	10	0.9991	0.001724	4.964×10^{-6}	348	579
IL-AC2900	2521	10	0.9999	0.001716	1.154×10^{-5}	149	579
IL-AC4700	3545	10	0.9976	0.001215	1.334×10^{-5}	92	814
IL-AC4800	3978	10	0.9995	0.001069	2.469×10^{-5}	44	914
IL-AC4900	3748	10	0.9985	0.001141	2.005×10^{-5}	58	861
IL-AC6700	2545	10	0.9998	0.001691	1.923×10^{-5}	89	585
IL-AC6800	3405	10	0.9998	0.001252	2.639×10^{-5}	49	782
IL-AC6900	3156	10	0.9996	0.001347	3.275×10^{-5}	42	725

Supplementary Table 2 Measures of porosity of IL-ACxT carbons. Classical measures (BET surface area (A_{BET}) and pore volume (V_{sp})), and NLDFT measurements, (NLDFT surface area (A_{NLDFT}) and NLDFT pore volume (V_{NLDFT})) are accompanied, in parenthesis, by the surface area or pore volume arising from micropores and the proportion taken up by micropores as a percentage of the total. The middle column shows the BETSI surface area.

Sample	**A_{BET} ($m^2 g^{-1}$)**	**V_{sp} ($cm^3 g^{-1}$)**	**BETSI surface area ($m^2 g^{-1}$)**	**A_{NLDFT} ($m^2 g^{-1}$)**	**V_{NLDFT} ($cm^3 g^{-1}$)**
IL-AC2700	1803 (1424, 79%)	0.81 (0.58, 72%)	1783	1489 (1421, 95%)	0.74 (0.65, 88%)
IL-AC2800	2619 (1853, 71%)	1.35 (0.80, 60%)	2519	1993 (1727, 87%)	1.23 (0.86, 70%)
IL-AC2900	2524 (1433, 57 %)	1.46 (0.66, 45%)	2521	1915 (1528, 80%)	1.33 (0.77, 58%)
IL-AC4700	3662 (1745, 48%)	2.23 (0.79, 35%)	3545	2391 (1661, 70%)	2.04 (0.96, 47%)
IL-AC4800	3995 (1223, 31%)	3.30 (0.81, 25%)	3978	2647 (1266, 48%)	3.07 (0.72, 24%)
IL-AC4900	3817 (1172, 31%)	2.97 (0.64, 22%)	3748	2547 (1365, 54%)	2.75 (0.76, 28%)
IL-AC6700	2567 (1322, 52%)	1.50 (0.60, 40%)	2545	1837 (1404, 76%)	1.37 (0.74, 54%)
IL-AC6800	3394 (1305, 38%)	2.40 (0.71, 30%)	3405	2244 (1280, 57%)	2.22 (0.73, 33%)
IL-AC6900	3135 (876, 28%)	2.81 (0.61, 22%)	3156	2131 (976, 46%)	2.63 (0.54, 21%)

Supplementary Table 3 Elemental composition of IL-C carbon compared to other carbonaceous precursors, namely, flash air-carbonised date seed (ACDS), flash air-carbonised sawdust (ACSD), flash air-carbonised cloves (ACSD), CNL1 carbon (CNL1), raw sawdust (SDD), cloves hydrochar (HCC), sawdust hydrochar (SD), lignin hydrochar (LAC), jujun grass hydrochar (ACGR), *Camelia Japonica* hydrochar (ACCA), cellulose hydrochar (C), cellulose acetate hydrochar (CA), starch hydrochar (S), fresh cigarette filter hydrochar (FF)), smoked cigarette filter hydrochar (SF), carbon nanotube composites (CN) and polypyrrole (Py). The references are from the main article.

Carbonaceous precursor	C [%]	H [%]	O [%]	(O/C)[a]	Reference
IL-C[b]	69.1	0.9	10.7	0.116	This work
Flash air carbonised date seed (ACDS)	78.5	4.0	16.3	0.156	14
Flash air carbonised sawdust (ACSD)	72.4	3.2	24.2	0.251	48
Flash air carbonised cloves (ACC)	66.1	4.3	27.7	0.310	47
CNL1 carbon (CNL1)	77.7	3.1	19.2	0.185	46
Raw sawdust (SDD)	46.4	5.8	47.8	0.773	53
Cloves hydrochar (HCC)	62.1	6.3	30.1	0.360	47
Sawdust hydrochar (SD)	57.4	5.6	37.0	0.483	19,49
Lignin hydrochar (LAC)	66.6	5.1	28.3	0.319	51
Jujun grass hydrochar (AGGR)	55.8	5.7	38.5	0.517	52
Camellia Japonica hydrochar (ACCA)	49.1	5.2	45.7	0.698	52
Cellulose hydrochar (C)	69.5	6.2	24.4	0.263	49,50
Cellulose acetate hydrochar (CA)	66.2	3.9	29.9	0.339	50
Starch hydrochar (S)	68.8	6.6	24.6	0.269	49
Fresh cigarette filter hydrochar (FF)	63.6	4.2	32.2	0.380	43
Smoked cigarette filter hydrochar (SF)[c]	68.5	5.7	24.8	0.272	43
Carbon nanotube composites (CN)[d]	45.1	1.5	52.6	0.875	54
Polypyrrole (Py)[e,f]	44.5	3.0	39.9	0.672	18

[a]Atomic ratio. [b]IL-C contains 19.3 wt% N. [c]Smoked cigarette filter hydrochar contains 1 wt% N. [d]The CNT composites contained 0.8 wt% N, and therefore a nominal O content of 52.6% obtained as O = 100-C-H-N, which gives O/C ratio of 0.875. [e]Polypyrrole contained 12.6 wt% N. [f]Polypyrrole has nominal O content of 39.9% obtained as O = 100-C-H-N, which gives O/C ratio of 0.672.

Supplementary Table 4 Textural properties and surface area density of IL-AC carbons activated at 800 ^{o}C and KOH/IL-C ratio of 4 compared to similarly activated carbons derived from a variety of carbonaceous precursors. See Supplementary Table 3 for description of the precursors. The references are from the main article.

Precursor	Sample	Surface area[a] ($m^2\ g^{-1}$)	Pore volume[b] ($cm^3\ g^{-1}$)	Surface area density ($m^2\ cm^{-3}$)	O/C ratio of precursor	Reference
IL-C	IL-AC4800	3995 (1223)	3.30 (0.81)	1211	0.116	This work
ACDS	ACDS4800	2609 (1825)	1.10 (0.70)	2372	0.156	14
ACSD	ACSD-4800	2610 (1892)	1.15 (0.74)	2270	0.251	48
ACC	ACC4800	3175 (2568)	1.65 (1.17)	1924	0.310	47
CNL1	CNL1-4800	2183 (1886)	1.05 (0.84)	2079	0.185	46
SDD	SD4800D	2980 (478)	2.10 (0.30)	1419	0.773	53
HCC	HCC4800	3116 (2190)	1.75 (0.98)	1781	0.360	47
SD	SD4800	2783 (694)	1.80 (0.36)	1546	0.483	19,49
LAC	LAC4800	3235 (1978)	1.77 (0.93)	1828	0.319	51
ACGR	ACGR4800	2957 (1578)	1.72 (0.75)	1719	0.517	52
ACCA	ACCA4800	3537 (2557)	1.85 (1.21)	1912	0.698	52
C	C-4800	2125 (1707)	0.98 (0.74)	2168	0.263	49,50
CA	CA-4800	2864 (2662)	1.32 (1.17)	2170	0.339	50
FF	FF-4800	4113 (2075)	1.87 (0.79)	2199	0.380	43
SF	SF-4800	2393 (1810)	1.09 (0.70)	2195	0.272	43
CN	CN4800	3802 (33)	2.98 (0.22)	1276	0.875	54
Py	Py4800	3450 (1910)	2.57 (1.22)	1342	0.672	18

The values in the parenthesis refer to: [a]micropore surface area and [b]micropore volume.

Supplementary Table 5 Textural properties and surface area density of IL-AC carbons activated at 700 ^{o}C and KOH/IL-C ratio of 4 compared to similarly activated carbons derived from a variety of carbonaceous precursors. See Supplementary Table 3 for description of the precursors. The references are from the main article.

|Precursor	Sample	Surface area[a] ($m^2\ g^{-1}$)	Pore volume[b] ($cm^3\ g^{-1}$)	Surface area density ($m^2\ cm^{-3}$)	O/C ratio of precursor	Reference
IL-C	IL-AC4700	3662 (1745)	2.23 (0.79)	1642	0.116	This work
ACDS	ACDS4700	2192 (1871)	0.93 (0.74)	2357	0.156	14
ACC	ACC4700	2773 (2431)	1.42 (1.01)	1953	0.310	47
CNL1	CNL1-4700	1280 (1191)	0.65 (0.56)	1969	0.185	46
HCC	HCC4700	2743 (2267)	1.35 (1.05)	2032	0.360	47
SD	SD4700	2252 (2088)	1.03 (0.91)	2186	0.483	19,49
LAC	LAC4700	2038 (1832)	1.00 (0.84)	2028	0.319	51
ACGR	ACGR4700	3144 (2753)	1.56 (1.23)	2015	0.517	52
ACCA	ACCA4700	2983 (2500)	1.50 (1.14)	1987	0.698	52
C	C-4700	2370 (2201)	1.08 (0.94)	2194	0.263	49,50
CA	CA-4700	3771 (3484)	1.75 (1.54)	2155	0.339	50
S	S4700	2194 (2082)	1.01 (0.92)	2172	0.269	49
FF	FF-4700	2803 (1901)	1.23 (0.73)	2279	0.380	43
SF	SF-4700	2512 (2019)	1.20 (0.91)	2093	0.272	43
CN	CN4700	3202 (1106)	2.14 (0.20)	1496	0.875	54
Py	Py4700	3568	2.46 (0.28)	1450	0.672	18

The values in the parenthesis refer to: [a]micropore surface area and [b]micropore volume.

Supplementary Table 6 Methane uptake of the best performing IL-AC carbons compared to selected benchmark MOFs and carbons. Volumetric uptake of powder MOFs is calculated based on crystallographic density rather than packing density.

Sample	Density ($g\ cm^{-3}$)	65 bar ($g\ g^{-1}$)	65 bar ($cm^3\ cm^{-3}$)	80 bar ($g\ g^{-1}$)	80 bar ($cm^3\ cm^{-3}$)	100 bar ($g\ g^{-1}$)	100 bar ($cm^3\ cm^{-3}$)	Reference
IL-AC4700	0.49	0.33	230	0.37	256	0.42	287	This work
IL-AC4800	0.39	0.41	223	0.46	253	0.53	289	This work
IL-AC4900	0.31	0.39	164	0.43	184	0.49	209	This work
CHCC2800	0.82	0.26	293	0.28	315	0.30	339	1
CHCC4700	0.75	0.27	282	0.29	306	0.32	334	1
CHCC4800	0.58	0.32	258	0.35	279	0.38	309	1
CNL4800	0.67	0.26	241	0.29	269	0.31	291	2
PPYCNL124	0.52	0.30	217	0.33	238	0.36	260	2
PPYCNL214	0.36	0.36	183	0.41	204	0.46	229	2
ACDS4800	0.69	0.25	243	0.27	262	0.29	282	2,3
PPYSD114	0.47	0.32	211	0.35	231	0.39	254	3
AX-21 carbon	0.487	0.30	203	0.33	222	0.35	238	4
HKUST-1	0.881	0.21	263	0.22	272	0.23	281	4
Ni-MOF-74	1.195	0.15	259	0.16	267	0.17	277	4
Al-soc-MOF-1	0.34	0.41	197	0.47	222			5
MOF-210	0.25	0.41	143	0.48	168			6
NU-1500-Al	0.498	0.29	200	0.31	216	0.34	237	7
NU-1501-Fe	0.299	0.40	168	0.46	193	0.52	218	7
NU-1501-Al	0.283	0.41	163	0.48	190	0.54	214	7
$_{mono}$HKUST-1	1.06	0.17	261	0.18	278	0.18	275	8
$_{mono}$UiO-66_D	1.05	0.14	210	0.17	245	0.20	296	9

References

1. I. Alali and R. Mokaya, *Energ Environ Sci*, 2022, **15**, 4710-4724.
2. A. Altwala and R. Mokaya, *Journal of Materials Chemistry A*, 2022, **10**, 13744-13757.
3. A. Altwala and R. Mokaya, *Energ Environ Sci*, 2020, **13**, 2967-2978.
4. J. A. Mason, M. Veenstra and J. R. Long, *Chemical Science*, 2014, **5**, 32-51.
5. D. Alezi, Y. Belmabkhout, M. Suyetin, P. M. Bhatt, L. J. Weselinski, V. Solovyeva, K. Adil, I. Spanopoulos, P. N. Trikalitis, A. H. Emwas and M. Eddaoudi, J Am Chem Soc, 2015, 137, 13308-13318.

6. H. Furukawa, N. Ko, Y. B. Go, N. Aratani, S. B. Choi, E. Choi, A. O. Yazaydin, R. Q. Snurr, M. O'Keeffe, J. Kim and O. M. Yaghi, Science, 2010, 329, 424-428.
7. Z. Chen, P. Li, R. Anderson, X. Wang, X. Zhang, L. Robison, L. R. Redfern, S. Moribe, T. Islamoglu, D. A. Gomez-Gualdron, T. Yildirim, J. F. Stoddart and O. K. Farha, *Science*, 2020, **368**, 297-303.
8. T. Tian, Z. Zeng, D. Vulpe, M. E. Casco, G. Divitini, P. A. Midgley, J. Silvestre-Albero, J. C. Tan, P. Z. Moghadam and D. Fairen-Jimenez, *Nat Mater*, 2018, **17**, 174-179.
9. B. M. Connolly, M. Aragones-Anglada, J. Gandara-Loe, N. A. Danaf, D. C. Lamb, J. P. Mehta, D. Vulpe, S. Wuttke, J. Silvestre-Albero, P. Z. Moghadam, A. E. H. Wheatley and D. Fairen-Jimenez, *Nat Commun*, 2019, **10**, 2345.

Supplementary Table 7 Methane uptake working capacity of the best performing IL-AC carbons compared to selected benchmark MOFs and carbons.

Sample	65 bar (g g^{-1})	65 bar (cm^3 cm^{-3})	80 bar (g g^{-1})	80 bar (cm^3 cm^{-3})	100 bar (g g^{-1})	100 bar (cm^3 cm^{-3})	Reference
IL-AC4700	0.27	184	0.30	210	0.36	241	This work
IL-AC4800	0.34	182	0.39	212	0.46	248	This work
IL-AC4900	0.31	132	0.35	151	0.41	177	This work
CHCC2800	0.18	200	0.20	222	0.22	246	1
CHCC4700	0.20	210	0.22	234	0.25	262	1
CHCC4800	0.25	197	0.28	218	0.31	248	1
CNL4800	0.19	182	0.22	202	0.24	224	2
PPYCNL124	0.23	167	0.26	188	0.29	209	2
PPYCNL214	0.29	146	0.34	167	0.39	192	2
ACDS4800	0.18	171	0.20	189	0.22	209	2,3
PPYSD114	0.25	162	0.28	182	0.32	205	2
AX-21 carbon	0.23	155	0.26	174	0.28	190	4
HKUST-1	0.15	179	0.16	198	0.17	207	4
Ni-MOF-74	0.08	148	0.09	152	0.10	162	4
Al-soc-MOF-1	0.36	176	0.42	201			5
MOF-210	0.38	134	0.45	157			6
NU-1500-Al	0.24	165	0.26	181	0.29	202	7
NU-1501-Fe	0.36	151	0.42	176	0.48	201	7
NU-1501-Al	0.37	147	0.44	174	0.50	198	7
$_{mono}$HKUST-1	0.12	184	0.13	201	0.13	198	8
$_{mono}$UiO-66_D	0.11	167	0.14	202	0.17	253	9

References

1. I. Alali and R. Mokaya, *Energ Environ Sci*, 2022, **15**, 4710-4724.
2. A. Altwala and R. Mokaya, *Journal of Materials Chemistry A*, 2022, **10**, 13744-13757.
3. A. Altwala and R. Mokaya, *Energ Environ Sci*, 2020, **13**, 2967-2978.
4. J. A. Mason, M. Veenstra and J. R. Long, *Chemical Science*, 2014, **5**, 32-51.
5. D. Alezi, Y. Belmabkhout, M. Suyetin, P. M. Bhatt, L. J. Weselinski, V. Solovyeva, K. Adil, I. Spanopoulos, P. N. Trikalitis, A. H. Emwas and M. Eddaoudi, J Am Chem Soc, 2015, 137, 13308-13318.
6. H. Furukawa, N. Ko, Y. B. Go, N. Aratani, S. B. Choi, E. Choi, A. O. Yazaydin, R. Q. Snurr, M. O'Keeffe, J. Kim and O. M. Yaghi, Science, 2010, 329, 424-428.
7. Z. Chen, P. Li, R. Anderson, X. Wang, X. Zhang, L. Robison, L. R. Redfern, S. Moribe, T.

Islamoglu, D. A. Gomez-Gualdron, T. Yildirim, J. F. Stoddart and O. K. Farha, *Science*, 2020, **368**, 297-303.
8. T. Tian, Z. Zeng, D. Vulpe, M. E. Casco, G. Divitini, P. A. Midgley, J. Silvestre-Albero, J. C. Tan, P. Z. Moghadam and D. Fairen-Jimenez, *Nat Mater*, 2018, **17**, 174-179.
9. B. M. Connolly, M. Aragones-Anglada, J. Gandara-Loe, N. A. Danaf, D. C. Lamb, J. P. Mehta, D. Vulpe, S. Wuttke, J. Silvestre-Albero, P. Z. Moghadam, A. E. H. Wheatley and D. Fairen-Jimenez, *Nat Commun*, 2019, **10**, 2345.

Supplementary Table 8 Elemental composition of carbonised ionic liquid (IL-C), air-carbonised date seed (ACDS) and polypyrrole (PPY).

Sample	C [%]	H [%]	N [%]	O [%]	(O/C)[a]	(C/N)[a]
IL-C	69.1	0.9	19.3	10.7	0.116	4.18
ACDS	78.5	4.0	2.1	16.3	0.156	43.6
PPY	55.5	2.7	16.0	25.8	0.349	4.04

[a]Atomic ratio.

Supplementary Table 9 Textural properties of IL-AC4800 compared to similarly activated carbons prepared from other precursors; ACDS4800 from air-carbonised date seed (ACDS) and PPY4800 from polypyrrole (PPY).

Sample	Surface area (m^2 g^{-1})	Micropore surface area[a] (m^2 g^{-1})	Pore volume (cm^3 g^{-1})	Micropore volume[b] (cm^3 g^{-1})	Packing density[c] (g cm^{-3})
IL-AC4800	3995	1523 (38)	3.30	0.81 (25)	0.39
ACDS4800	2609	1825 (70)	1.10	0.70 (63)	0.69
PPY4800	3279	1320 (40)	2.00	0.62 (31)	0.37

[a]Values in parenthesis are % of surface area from micropores. [b]Values in parenthesis are % of pore volume from micropores. [c]The packing density was determined by pressing a given amount of carbon in a 1.3 cm die at pressure of 7 MPa for 5 min.

Supplementary Table 10 Total gravimetric and volumetric methane uptake of IL-AC4800 compared to similarly activated carbons prepared from other precursors; ACDS4800 from air-carbonised date seed (ACDS) and PPY4800 from polypyrrole (PPY).

Sample	Total gravimetric ($g\ g^{-1}$) and volumetric (v/v)[a] methane uptake					
	35 bar		65 bar		100 bar	
	($g\ g^{-1}$)	(v/v)	($g\ g^{-1}$)	(v/v)	($g\ g^{-1}$)	(v/v)
IL-AC4800	0.28	156	0.41	223	0.53	289
ACDS4800	0.20	194	0.25	243	0.29	282
PPY4800	0.25	129	0.34	176	0.42	215

[a] Volumetric uptake (v/v) is given as cm^3 (STP) cm^{-3}

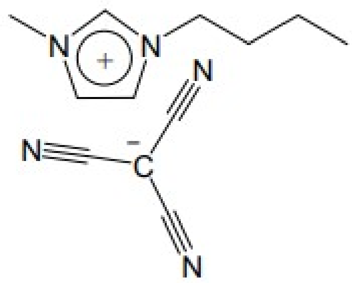

Supplementary Fig. 1 The chemical structure of Butyl-3-methylimidazolium tricyanomethanide ($C_{12}H_{15}N_5$), CAS number 878027-73-7.

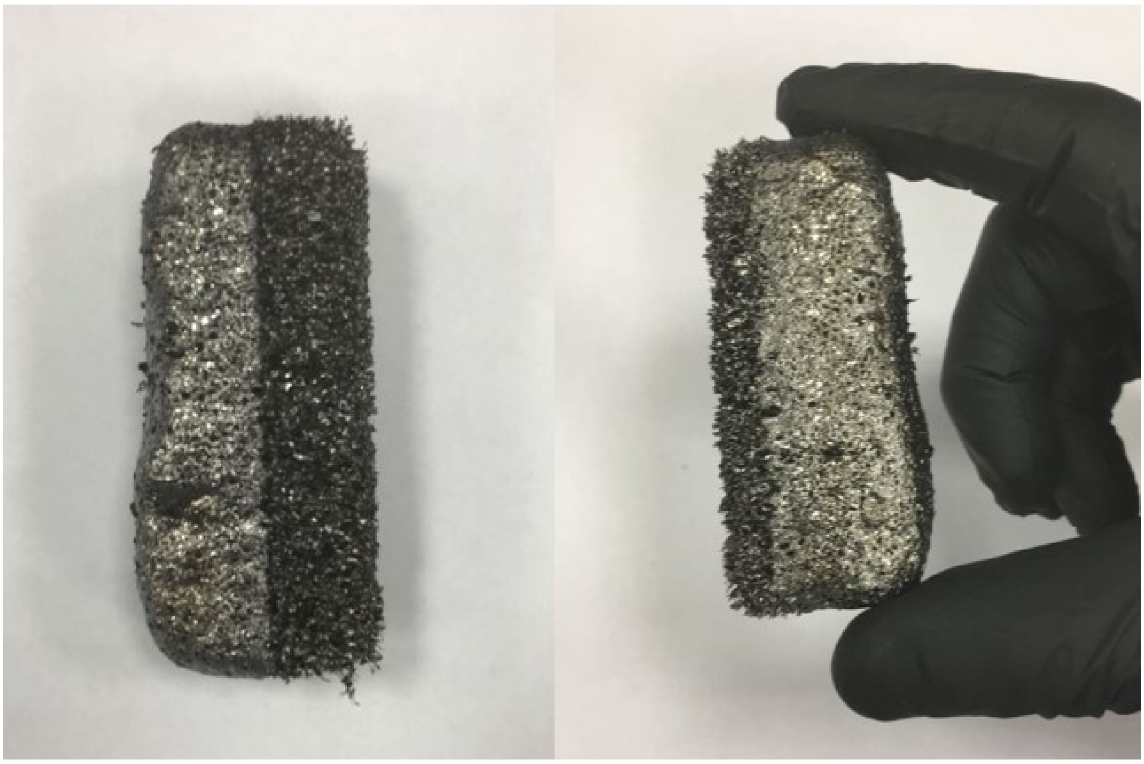

Supplementary Fig. 2 Photograph of the IL after carbonisation at 800 °C.

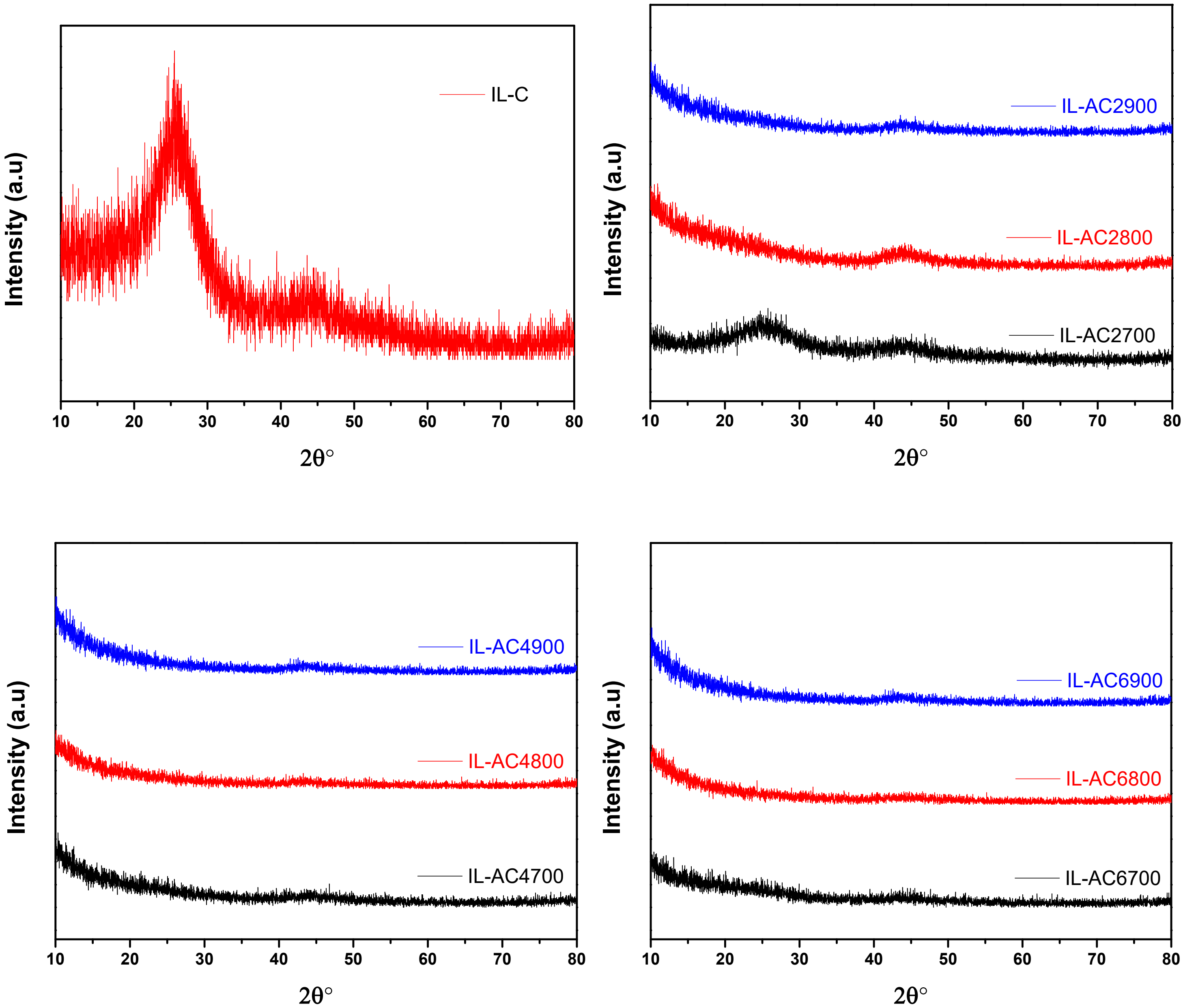

Supplementary Fig. 3 Powder XRD patterns of carbonised ionic liquid (IL-C) and IL-ACxT activated carbons prepared at KOH/IL-C ratio of 2, 4 or 6, and activation temperature of 700, 800 or 900 ^{o}C. (x = KOH/IL-C ratio, T is activation temperature).

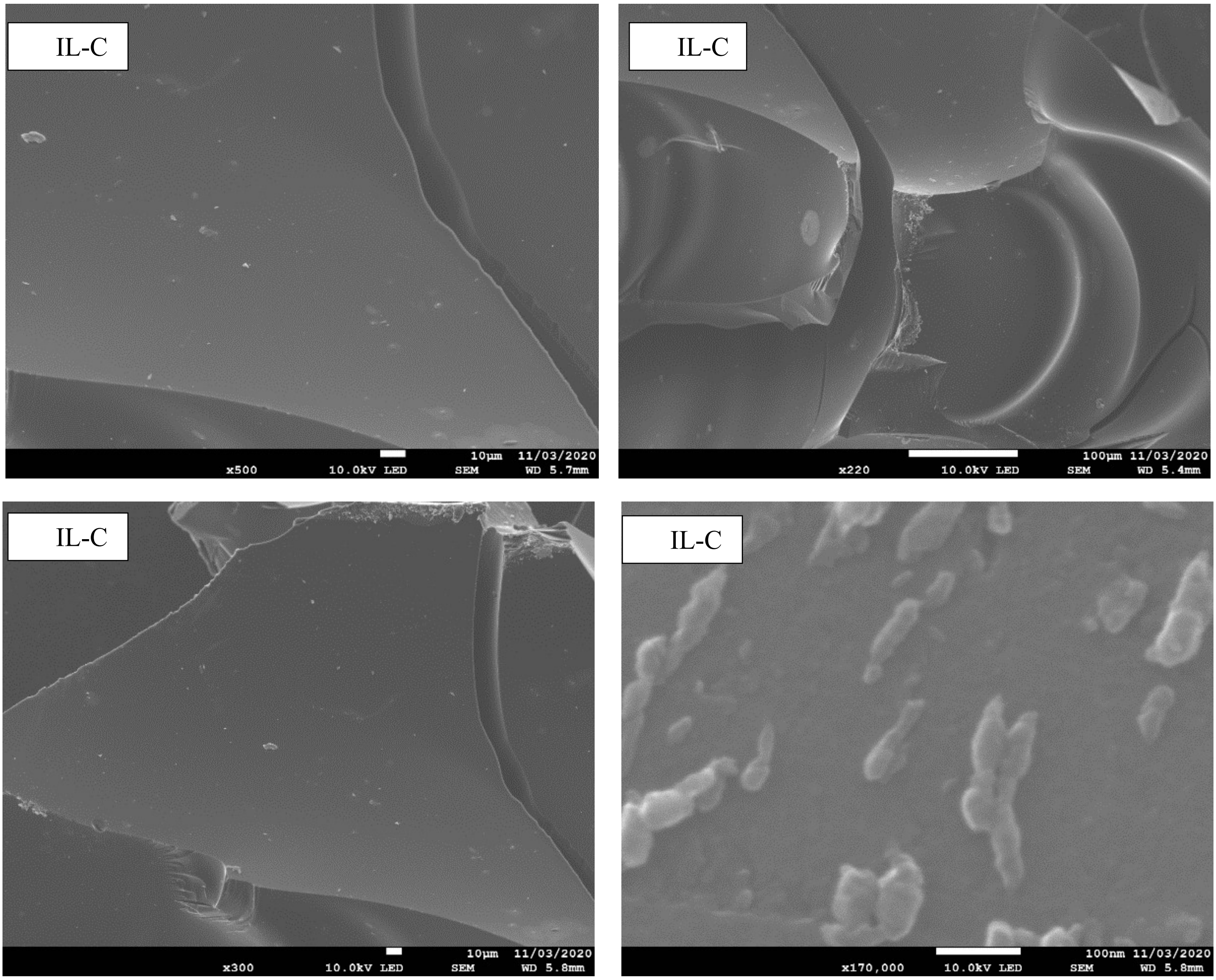

Supplementary Fig. 4 SEM images of the carbonised ionic liquid (IL-C).

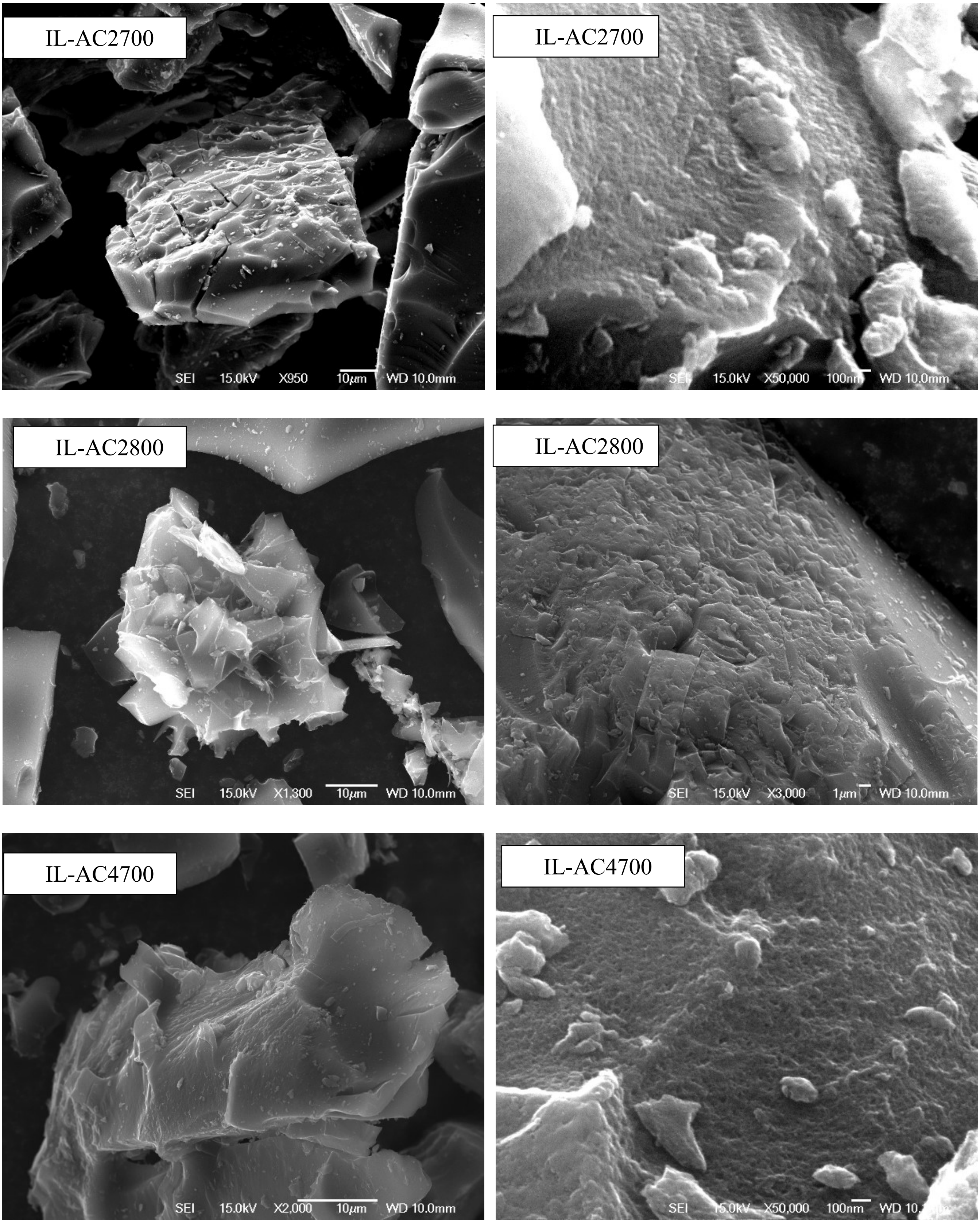

Supplementary Fig. 5 SEM images of the ionic liquid-derived activated carbons; IL-AC2700, IL-AC2800 and IL-AC4700.

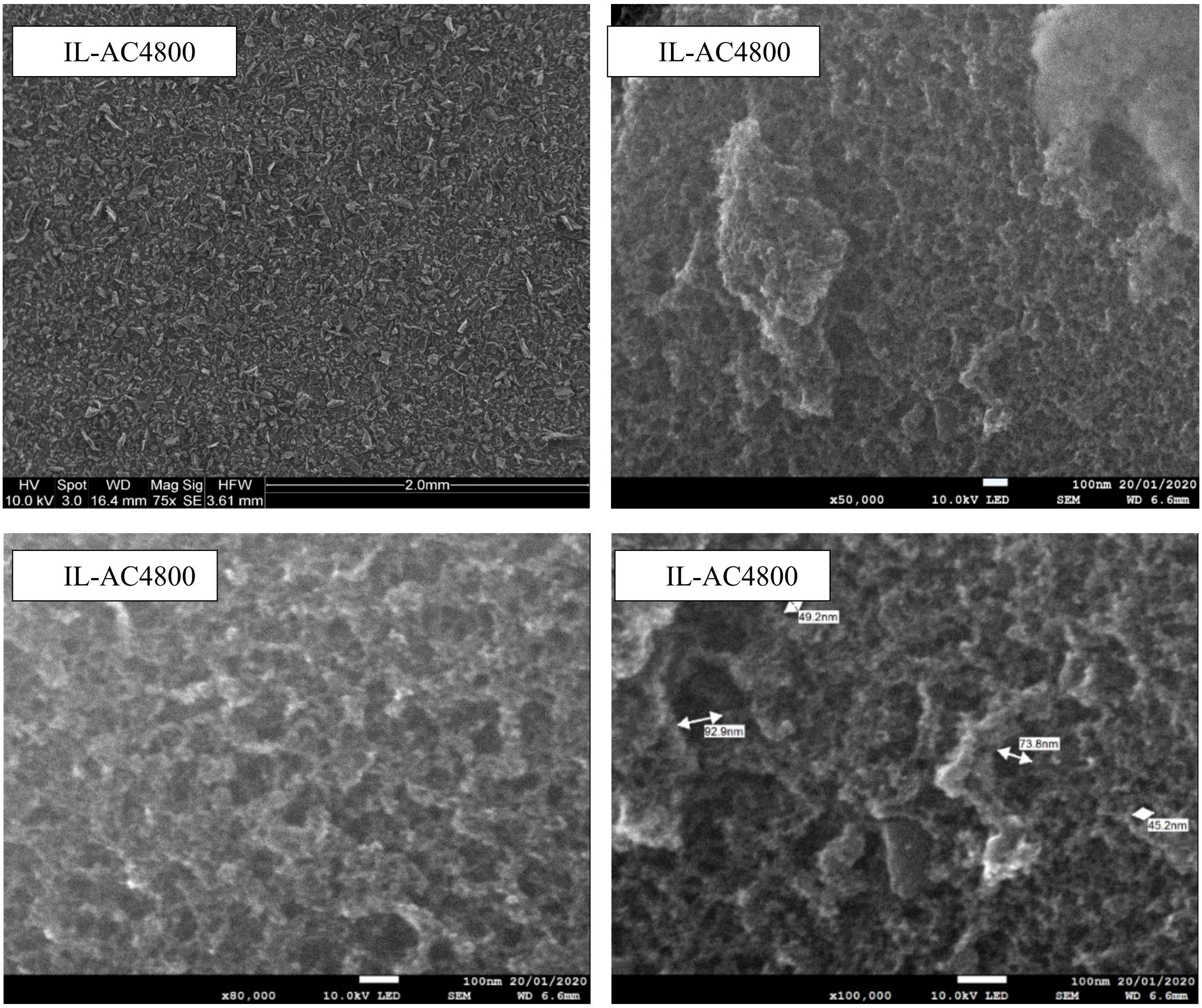

Supplementary Fig. 6 SEM images of the ionic liquid-derived activated carbon IL-AC4800.

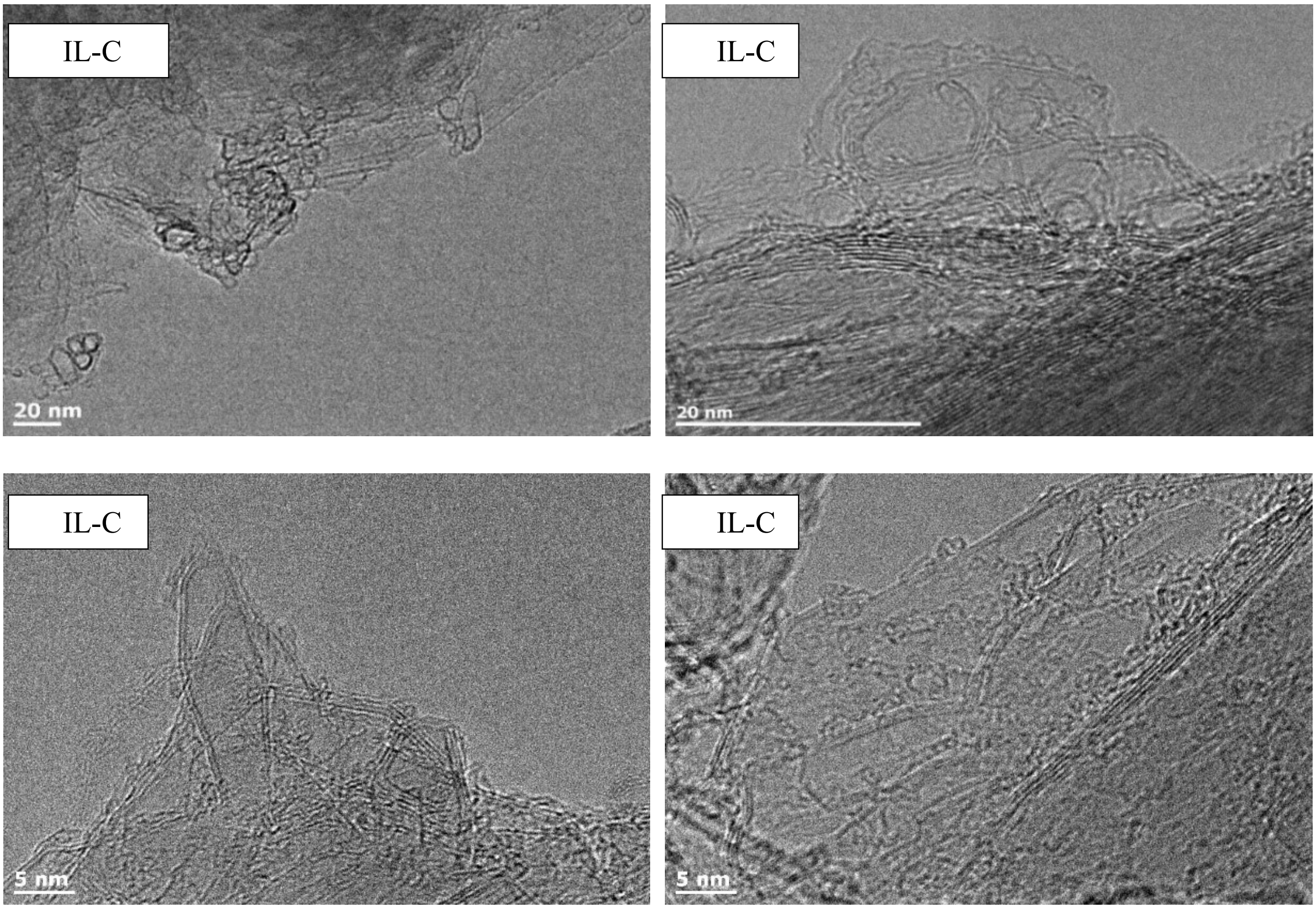

Supplementary Fig. 7 TEM images of carbonised ionic liquid (IL-C).

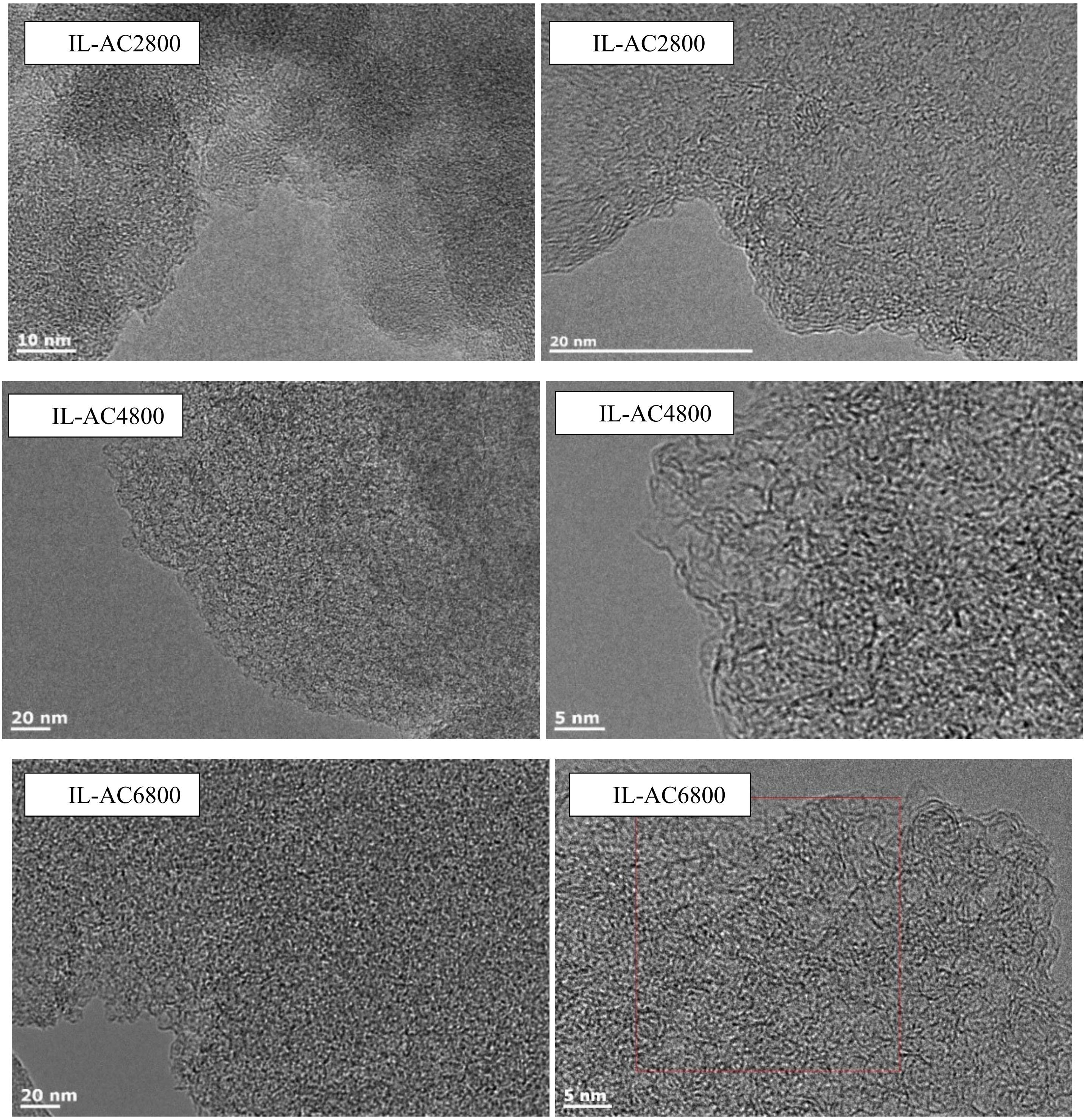

Supplementary Fig. 8 TEM images of activated carbons IL-AC2800, IL-AC4800 and IL-AC6800.

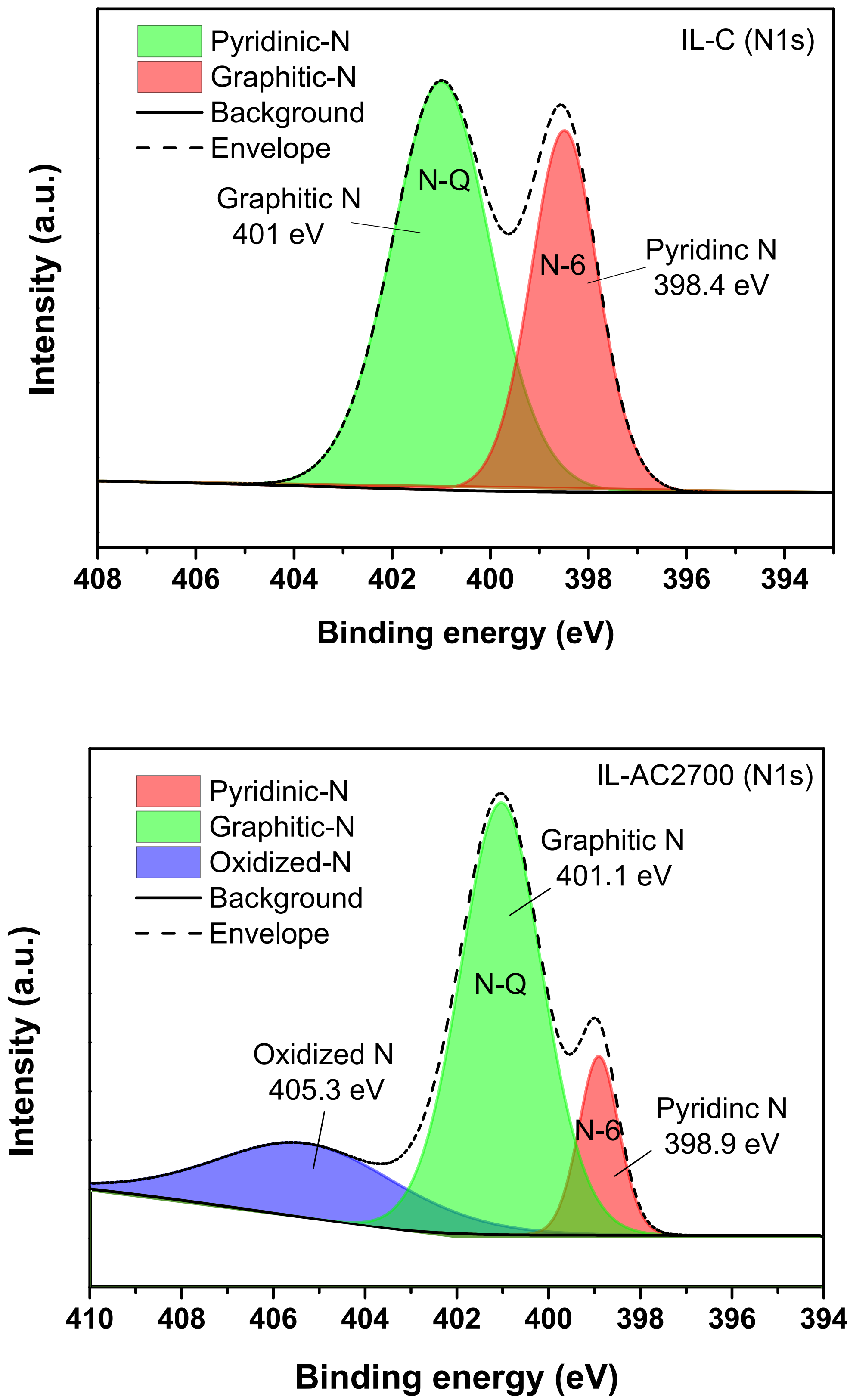

Supplementary Fig. 9 High-resolution XPS spectra showing N 1s peaks for carbonised ionic liquid (IL-C), and IL-AC2700 activated carbon.

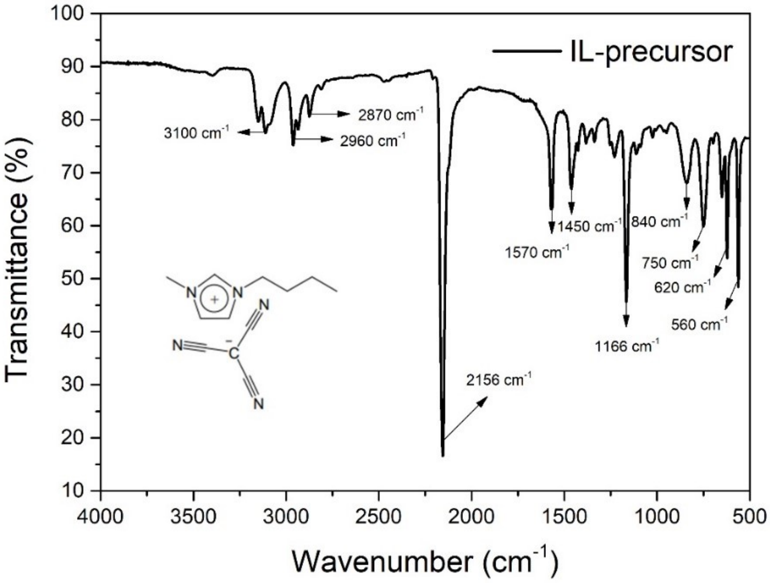

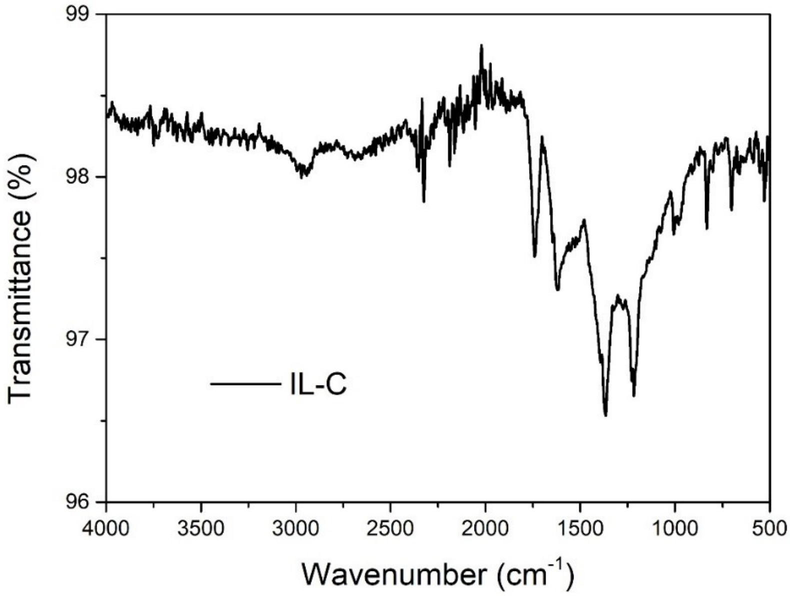

Supplementary Fig. 10 IR spectra of (top) 1-Butyl-3-methylimidazolium tricyanomethanide ionic liquid, and (bottom) the carbonised ionic liquid (IL-C).

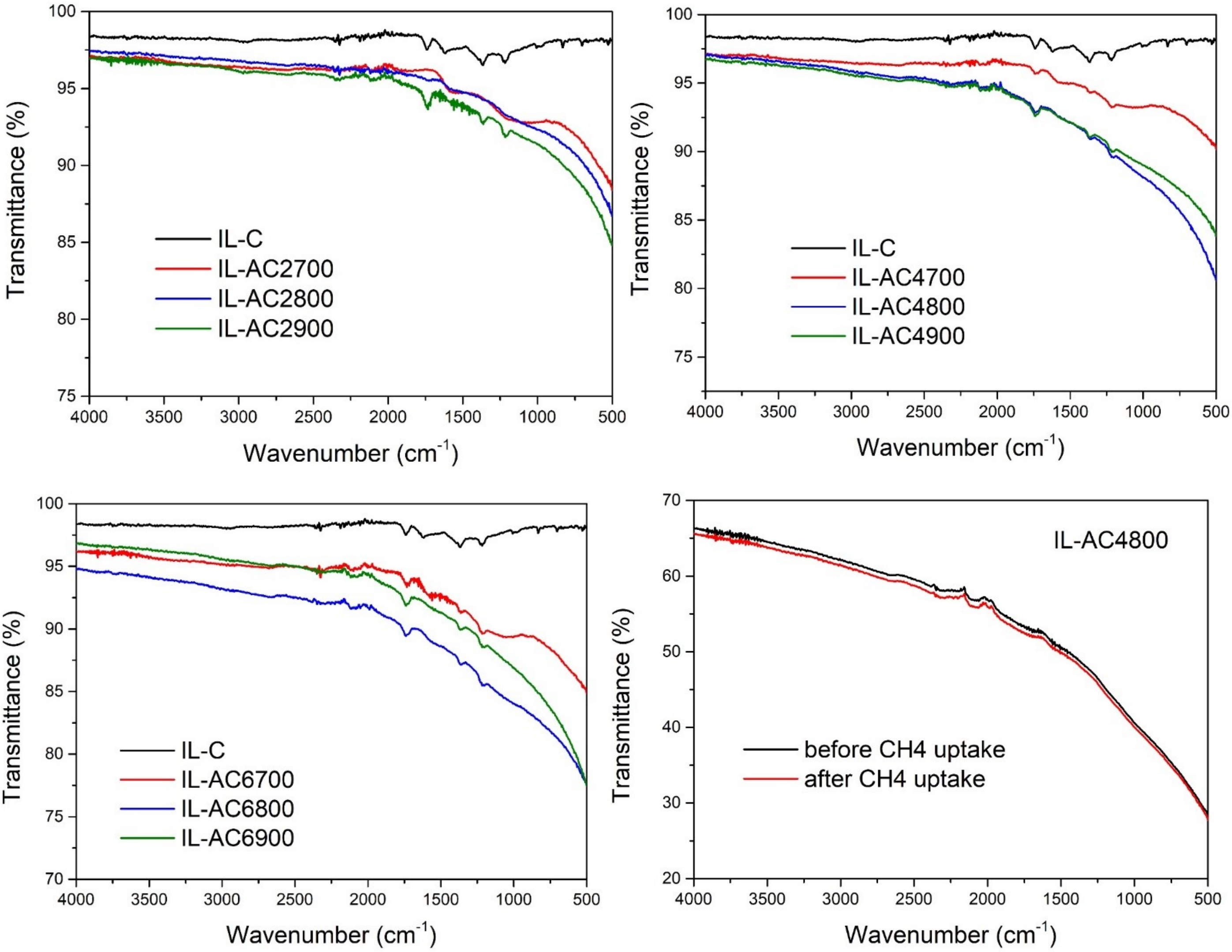

Supplementary Fig. 11 IR spectra of carbonised ionic liquid, IL-C, compared to that of IL-C derived activated carbon, IL-ACxT, where x is KOH/IL-C ratio (2,4 or 6), and T is activation temperature (700, 800 or 900 ^{o}C). A comparison of the IR spectra of sample IL-AC4800 before and after methane uptake is also shown.

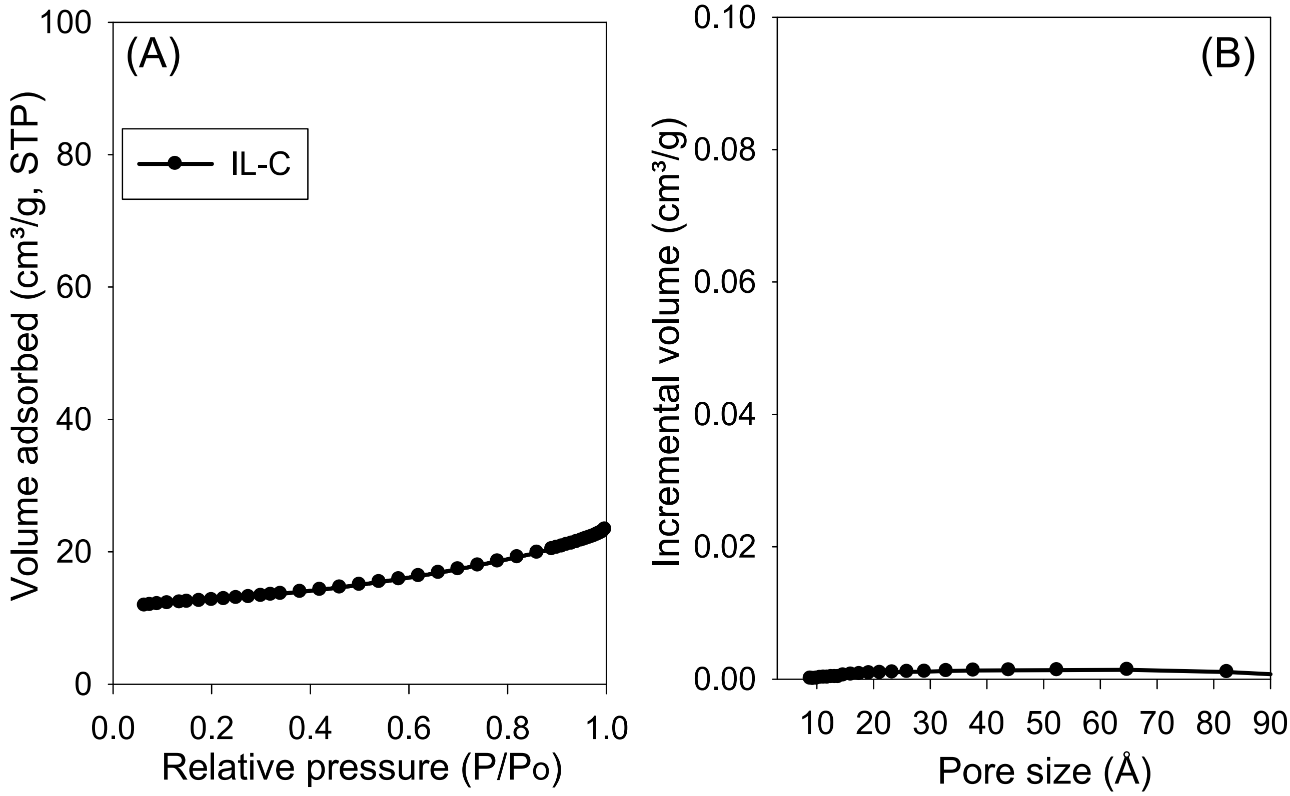

Supplementary Fig. 12 Nitrogen sorption isotherm (A) and pore size distribution curve (B) of carbonised ionic liquid (IL-C).

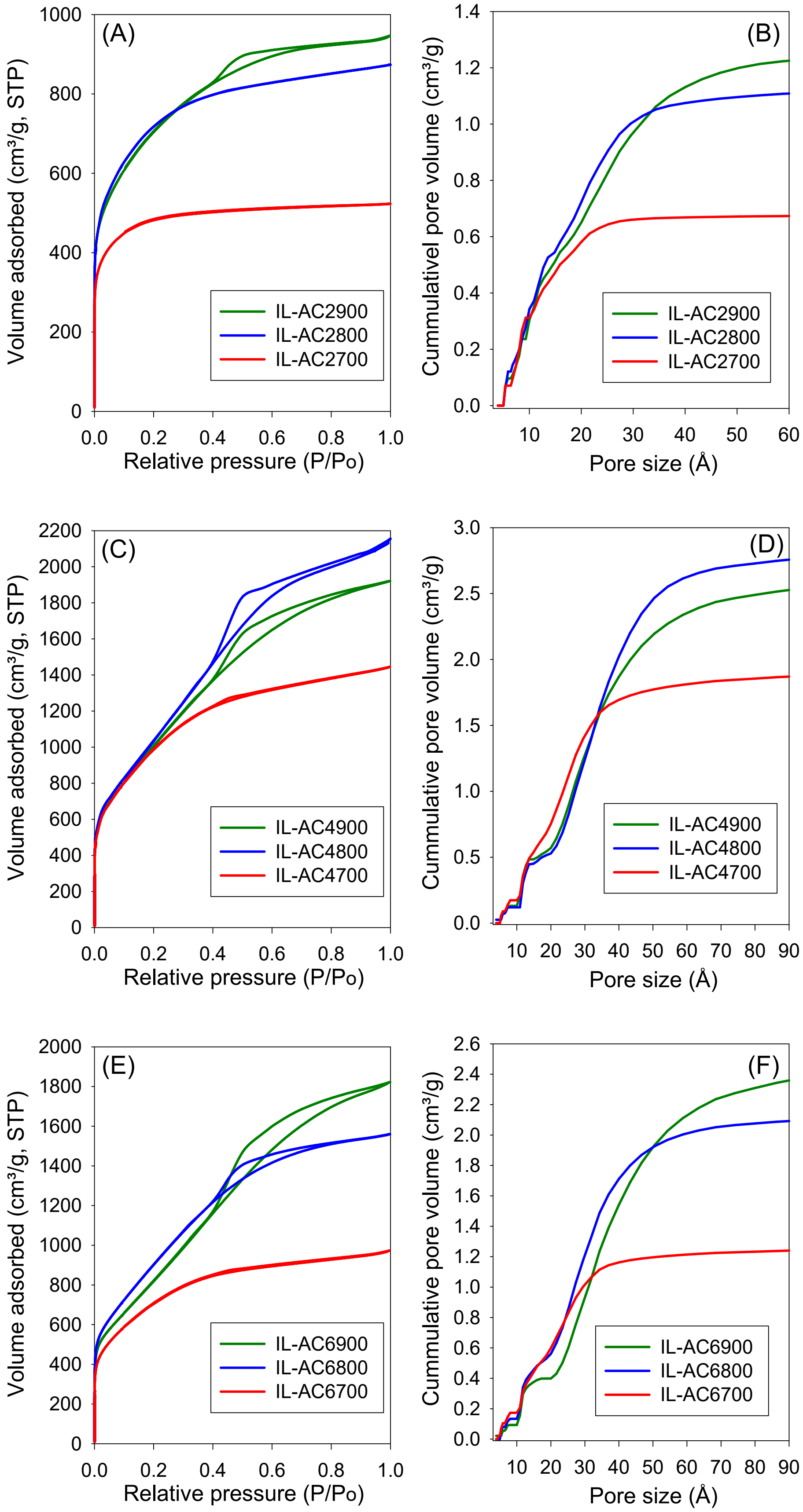

Supplementary Fig. 13 Nitrogen sorption isotherms (A, C and E) and cumulative pore size distribution curves (B, D and F)) of IL-ACxT carbons prepared at KOH/IL-C ratio of 2 (A, B), 4 (C, D) and 6 (E, F).

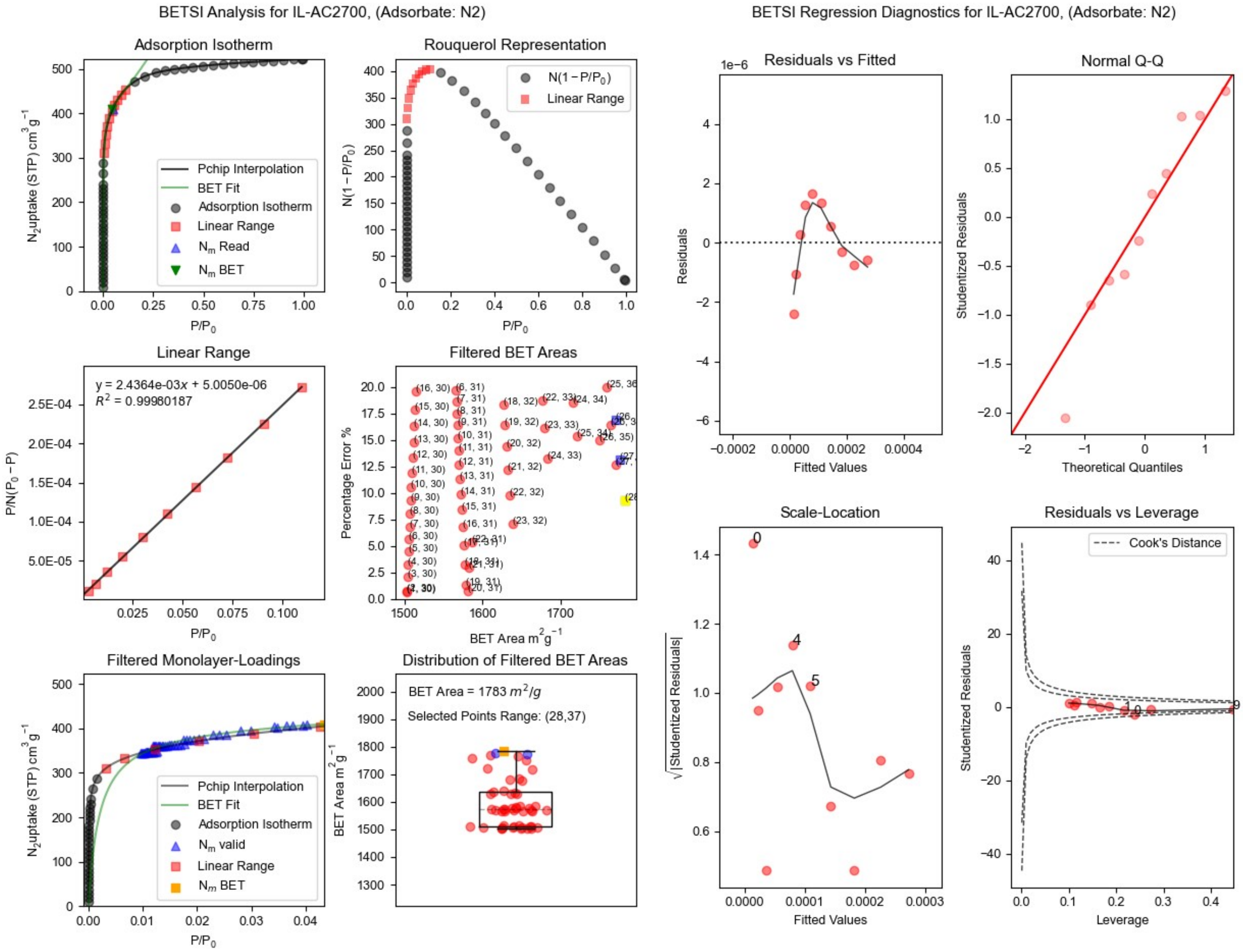

Supplementary Fig. 14 BETSI summary for sample IL-AC2700.

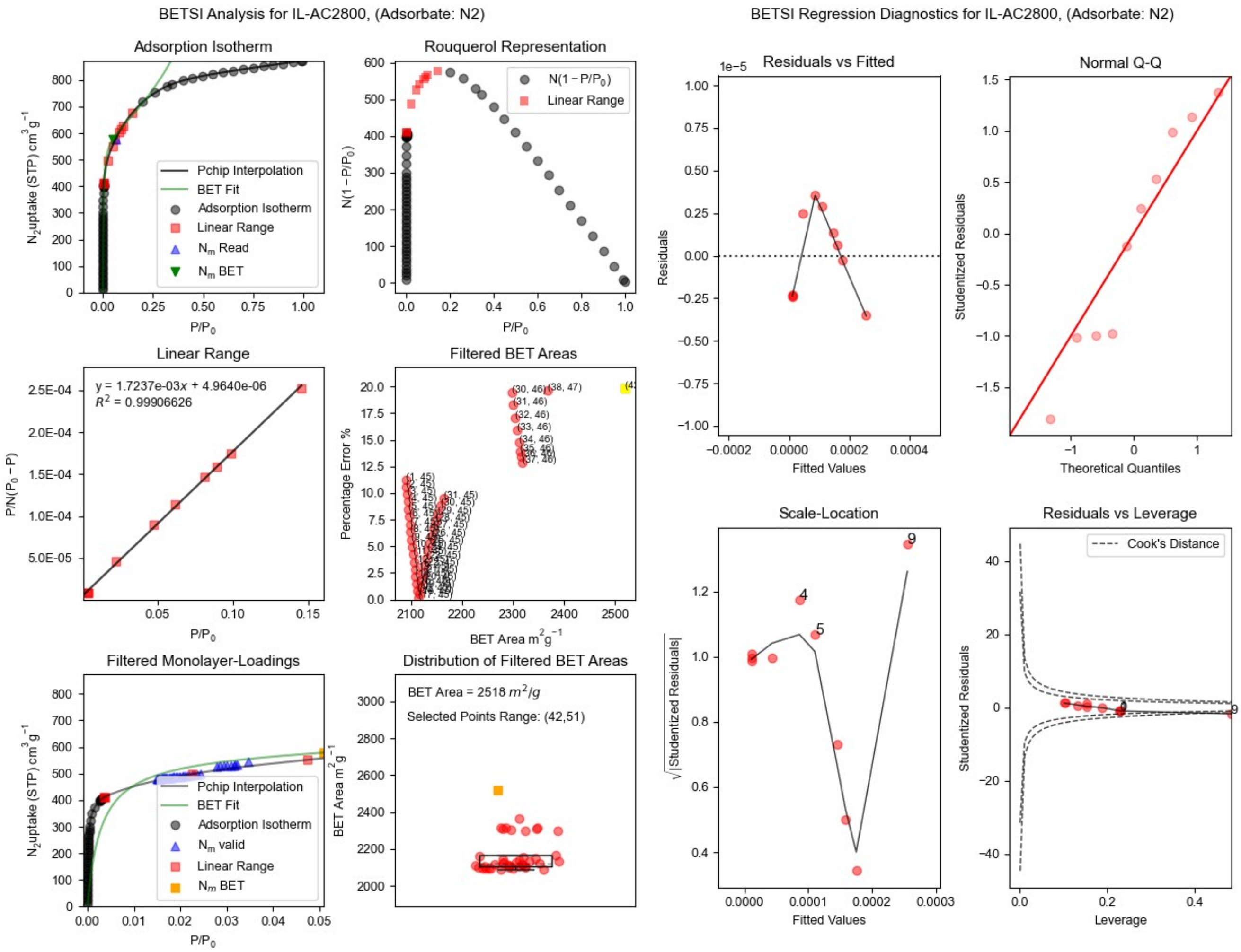

Supplementary Fig. 15 BETSI summary for sample IL-AC2800.

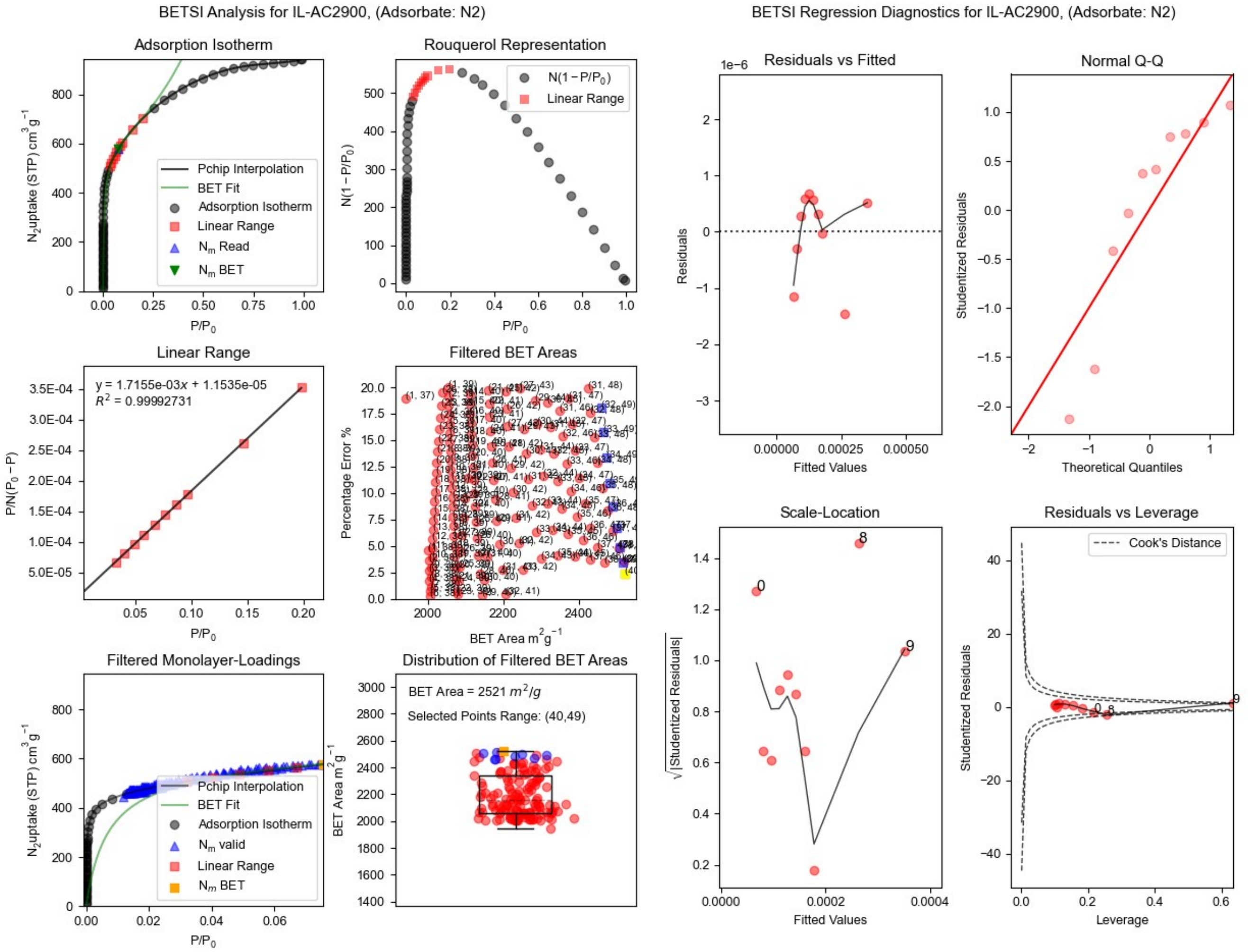

Supplementary Fig. 16 BETSI for summary sample IL-AC2900.

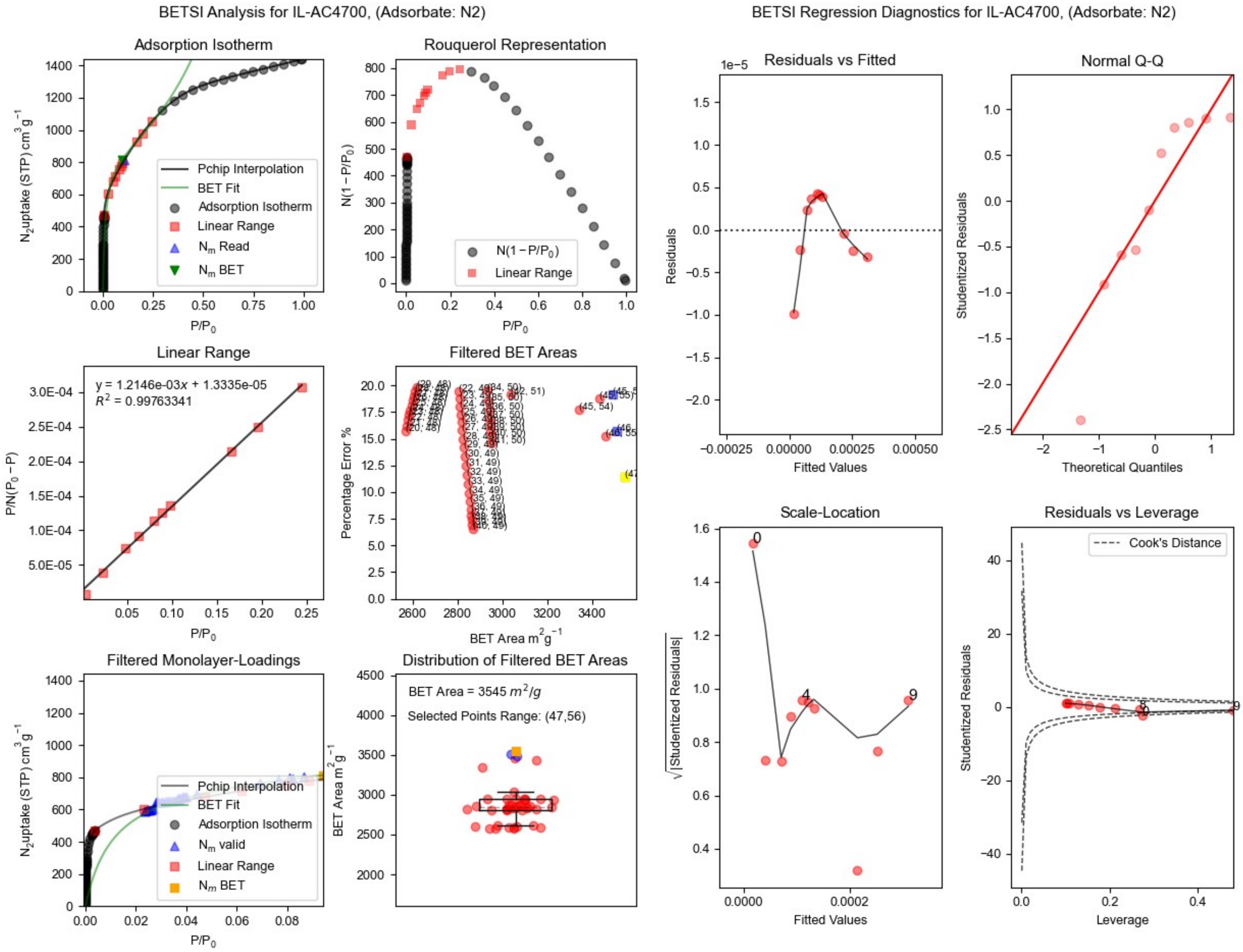

Supplementary Fig. 17 BETSI summary for sample IL-AC4700.

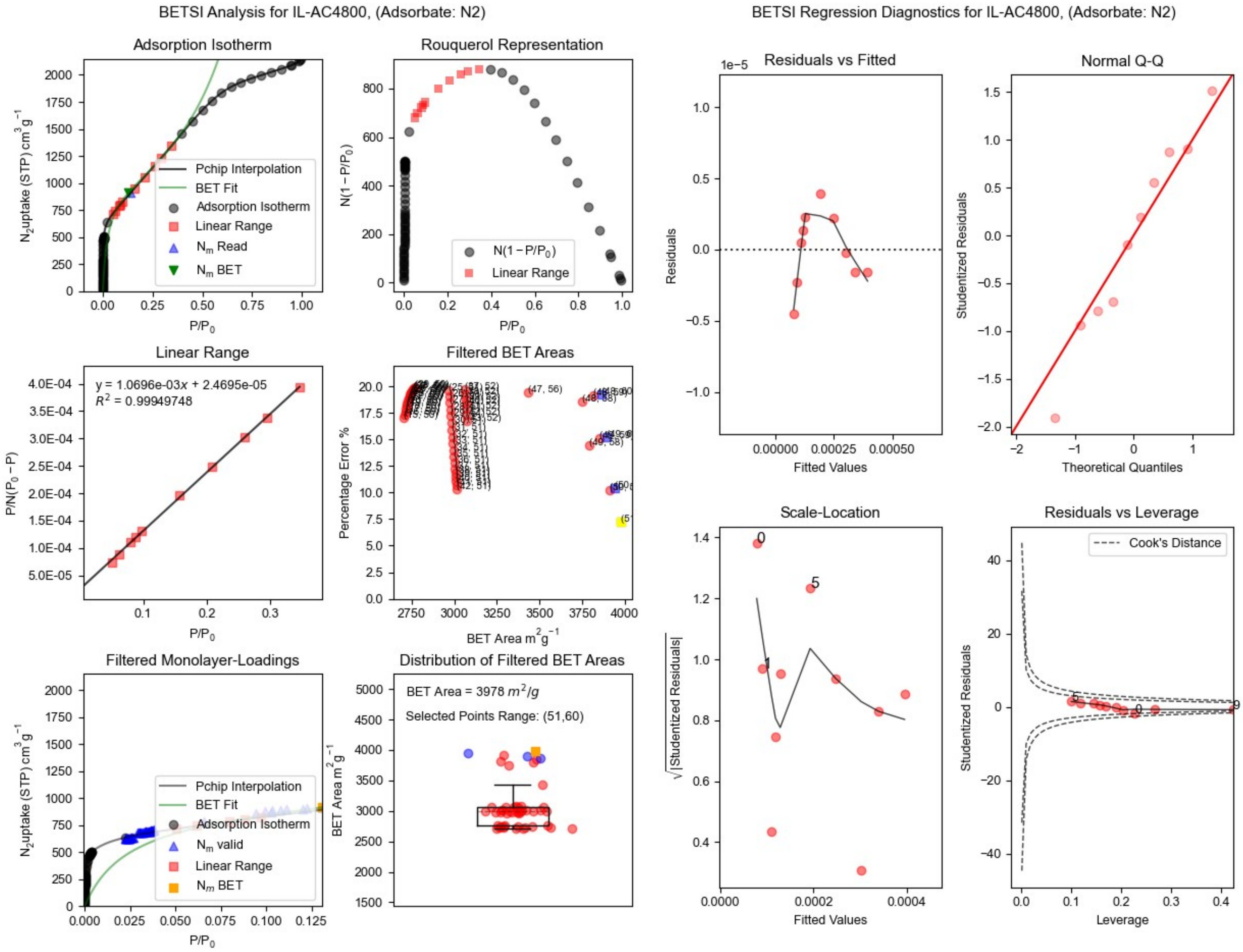

Supplementary Fig. 18 BETSI summary for sample IL-AC4800.

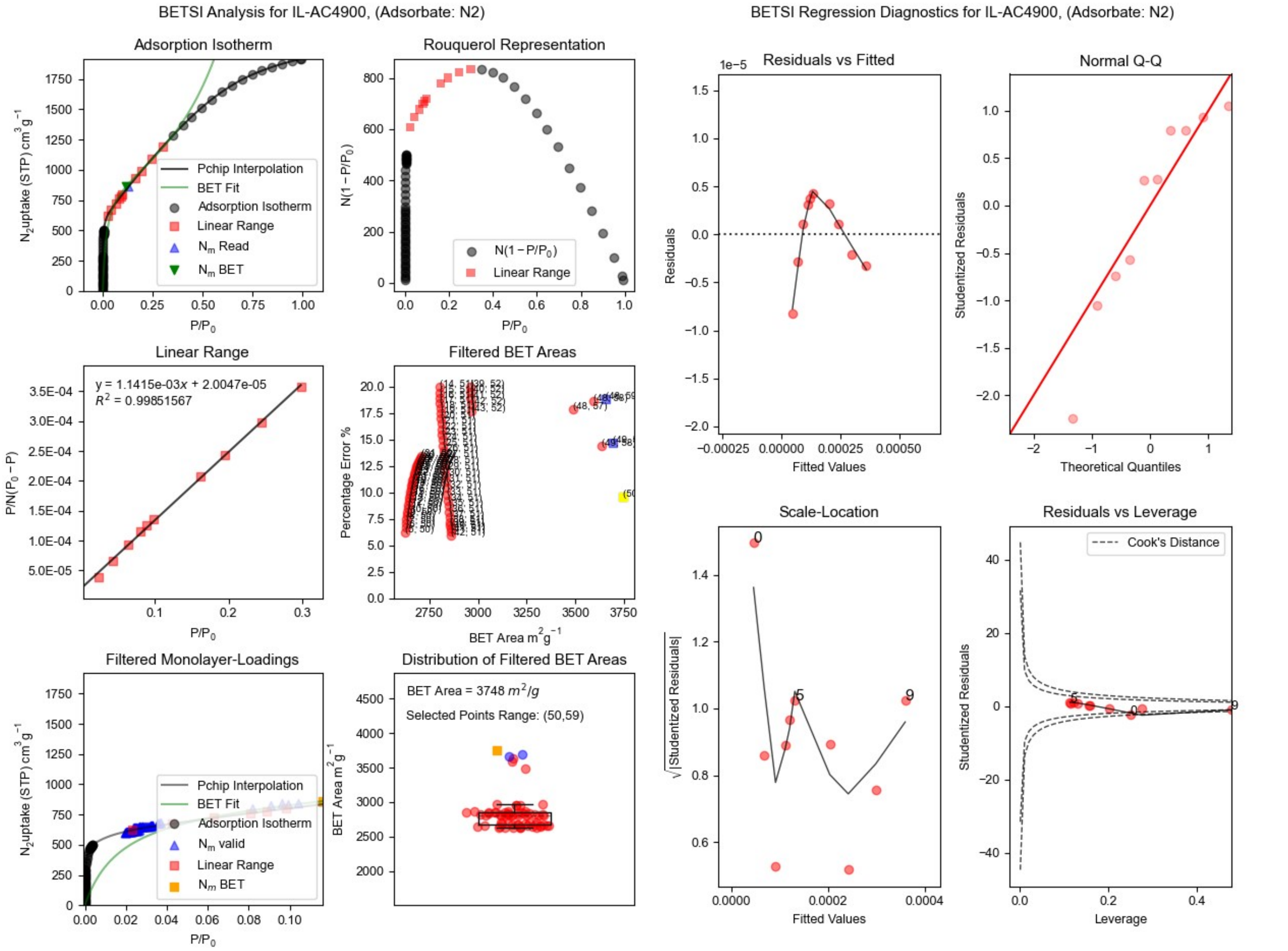

Supplementary Fig. 19 BETSI summary for sample IL-AC4900.

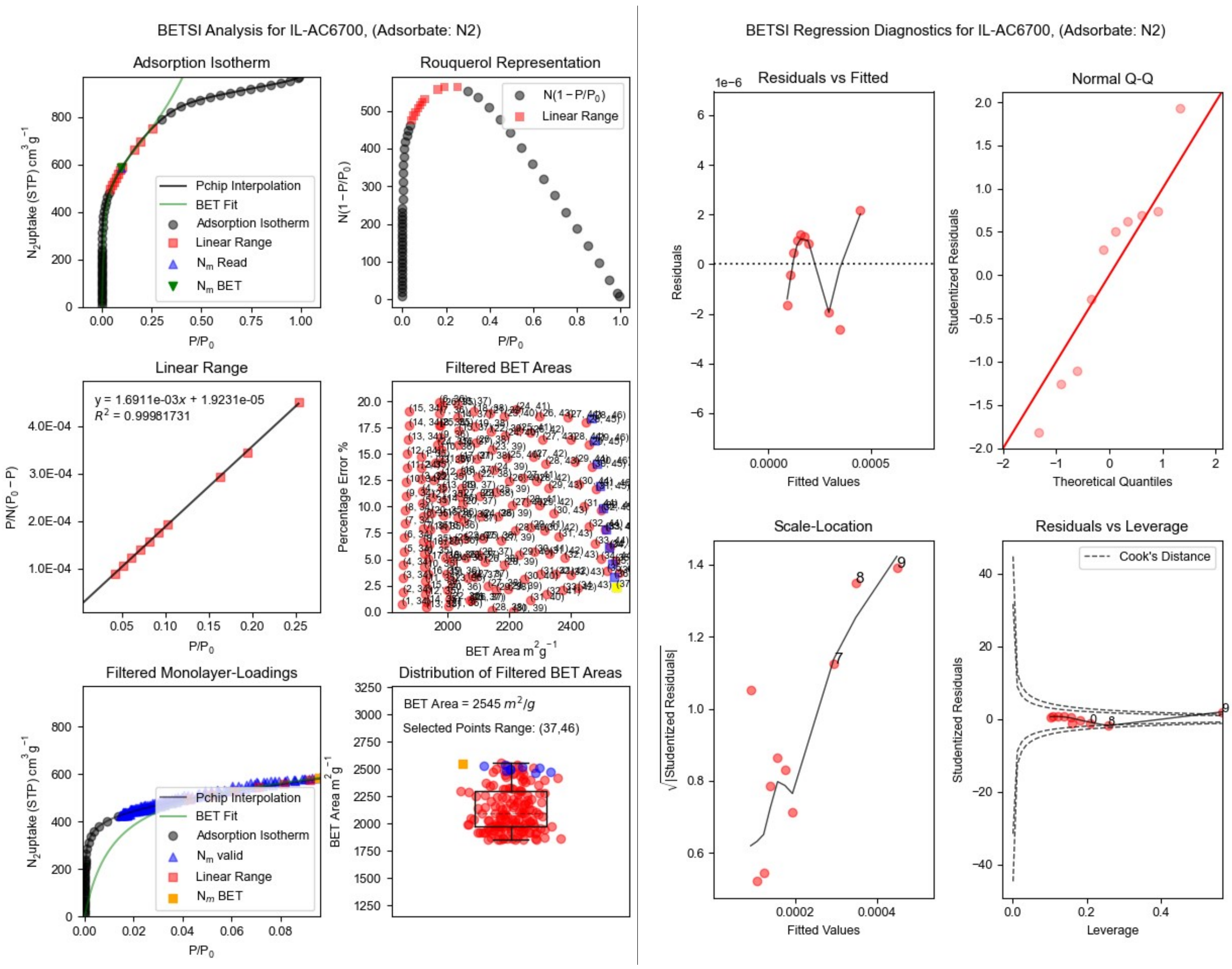

Supplementary Fig. 20 BETSI summary for sample IL-AC6700.

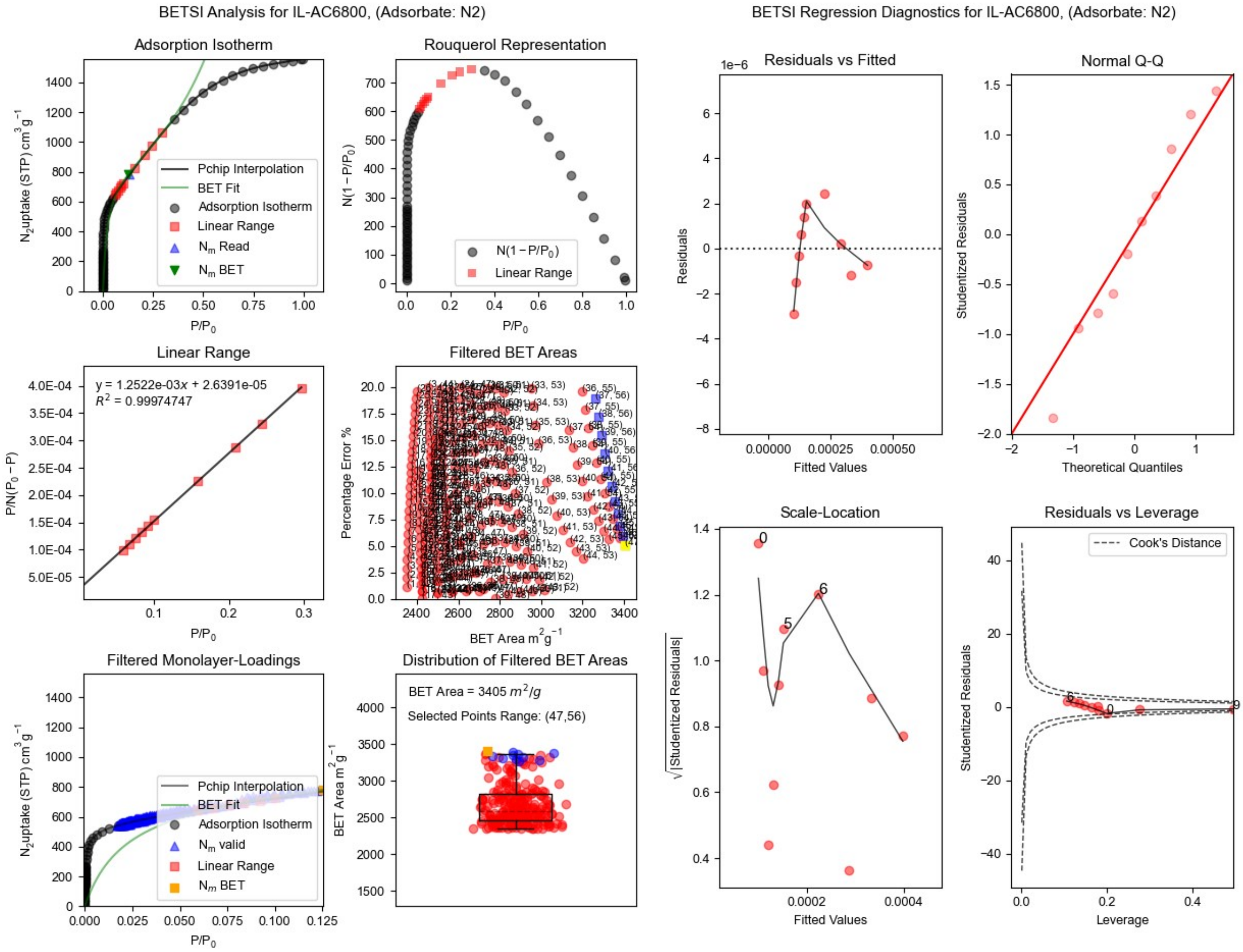

Supplementary Fig. 21 BETSI summary for sample IL-AC6800.

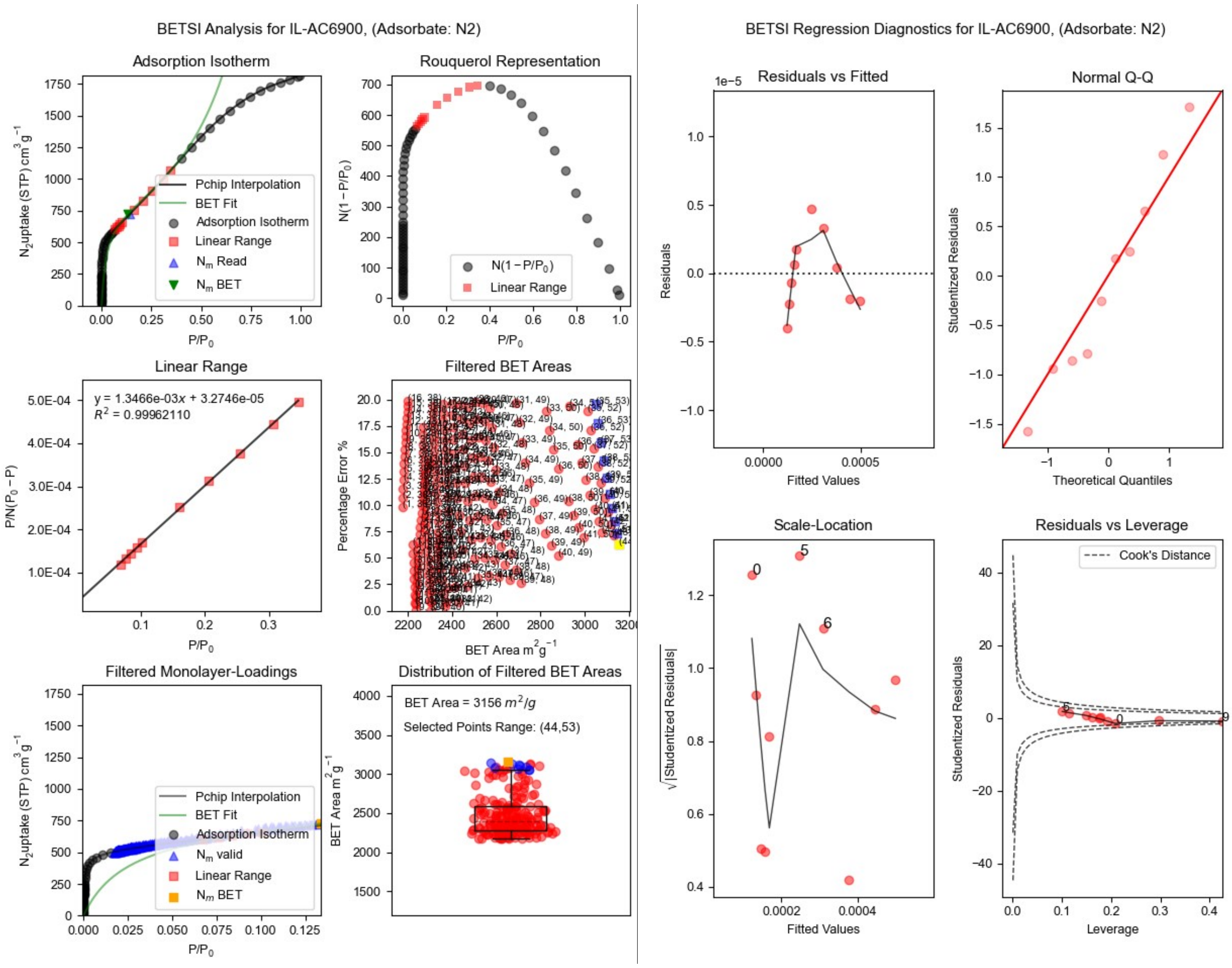

Supplementary Fig. 22 BETSI summary for sample IL-AC6900.

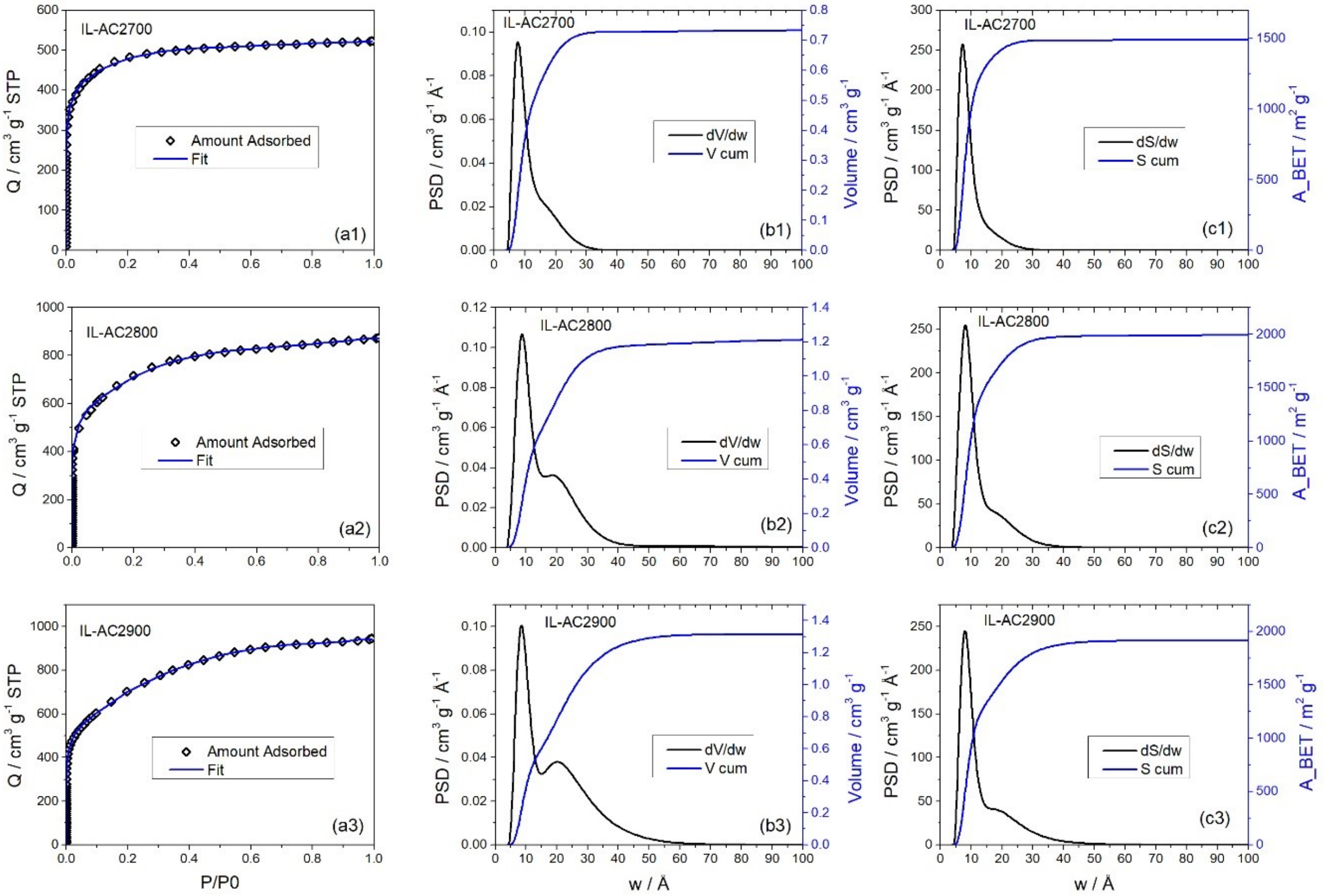

Supplementary Fig. 23 Nitrogen sorption isotherms and fits to the isotherms (column a), pore size distribution (PSD) curves and cumulative PSDs (column b), and PSD surface area and cumulative surface area (column c) derived via fitting to the 2D-NLDFT heterogeneous surface kernel for samples IL-AC2700 (top row), IL-AC2800 (middle row) and IL-AC2900 (bottom row).

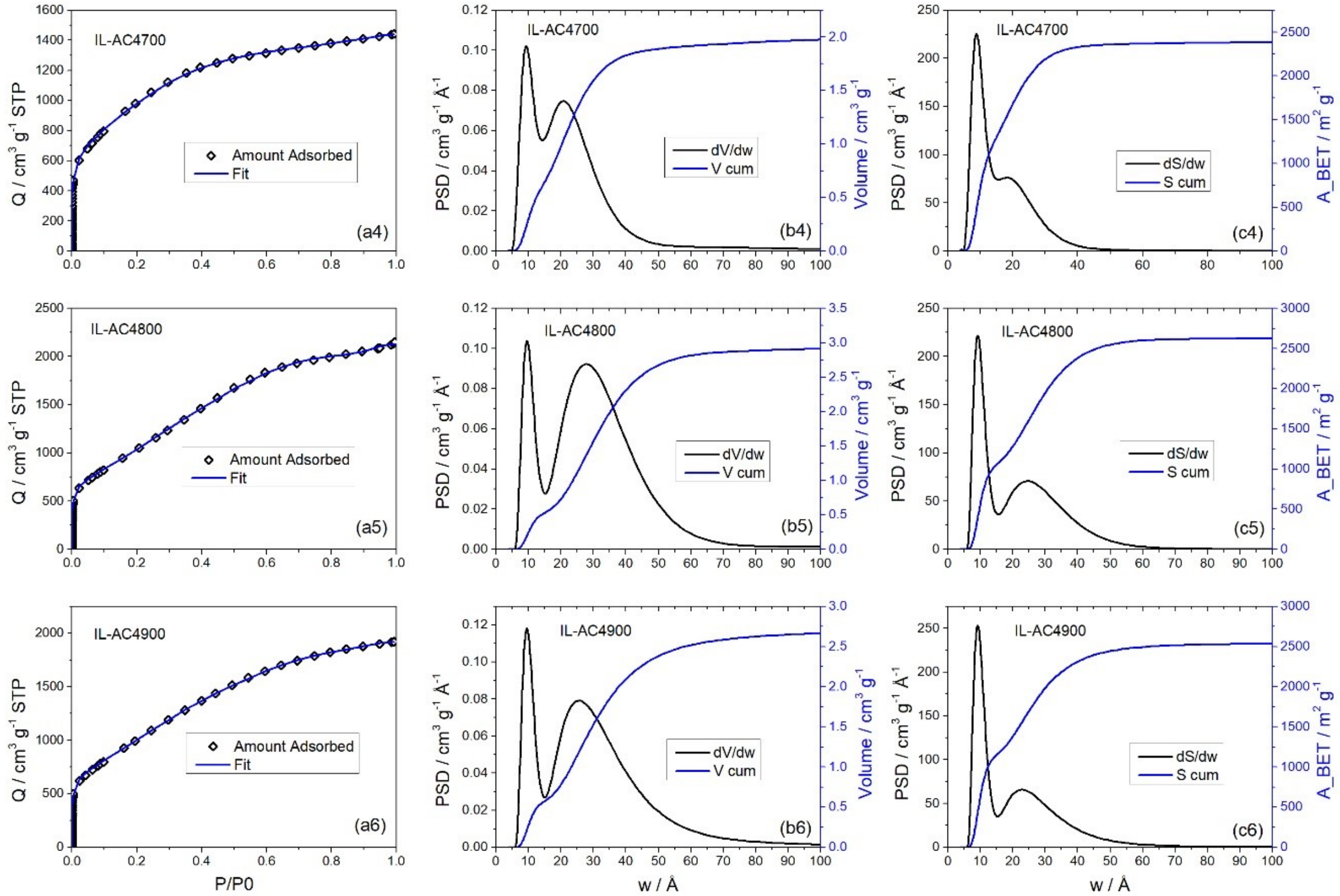

Supplementary Fig. 24 Nitrogen sorption isotherms and fits to the isotherms (column a), pore size distribution (PSD) curves and cumulative PSDs (column b), and PSD surface area and cumulative surface area (column c) derived via fitting to the 2D-NLDFT heterogeneous surface kernel for samples IL-AC4700 (top row), IL-AC4800 (middle row) and IL-AC4900 (bottom row).

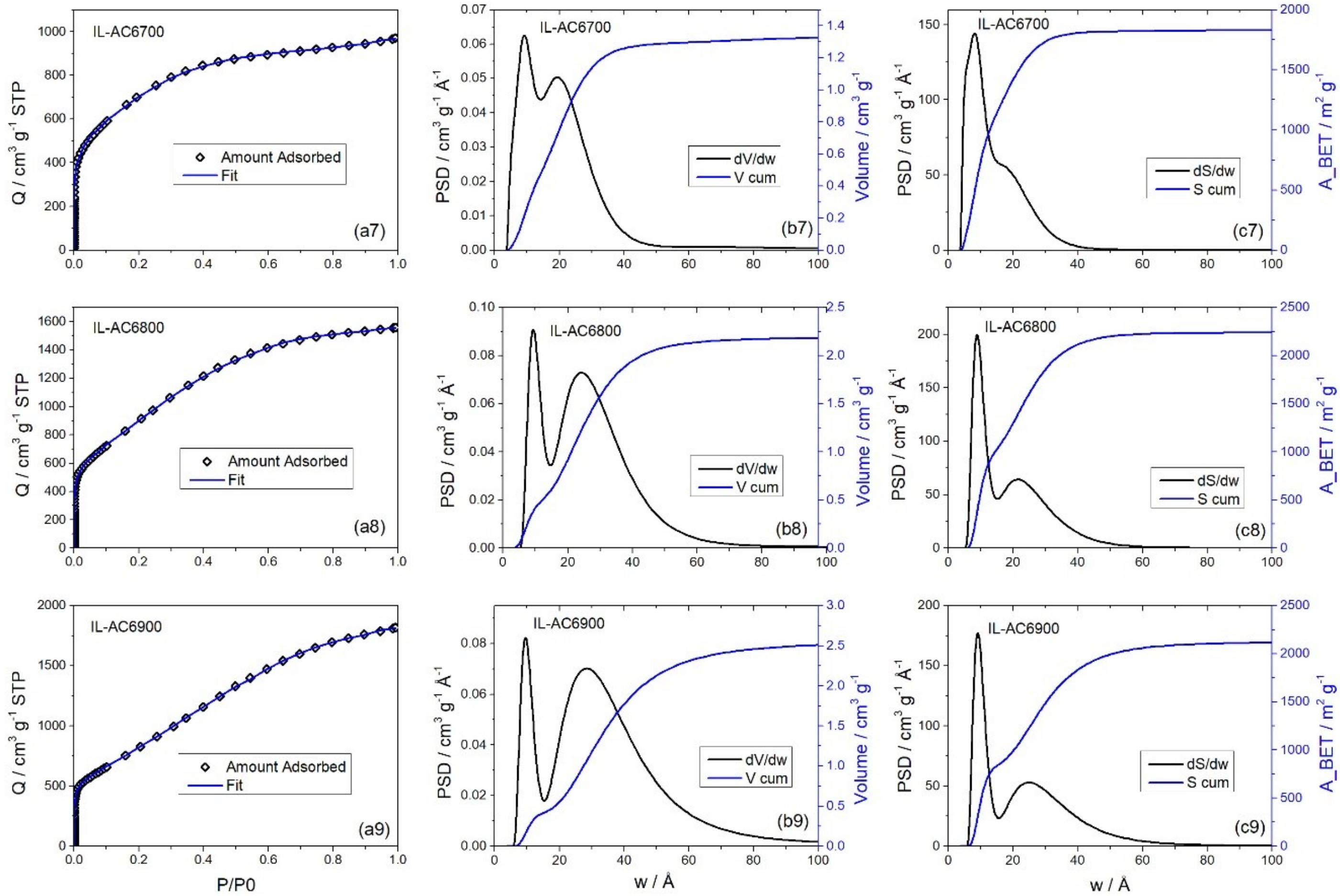

Supplementary Fig. 25 Nitrogen sorption isotherms and fits to the isotherms (column a), pore size distribution (PSD) curves and cumulative PSDs (column b), and PSD surface area and cumulative surface area (column c) derived via fitting to the 2D-NLDFT heterogeneous surface kernel for samples IL-AC6700 (top row), IL-AC6800 (middle row) and IL-AC6900 (bottom row).

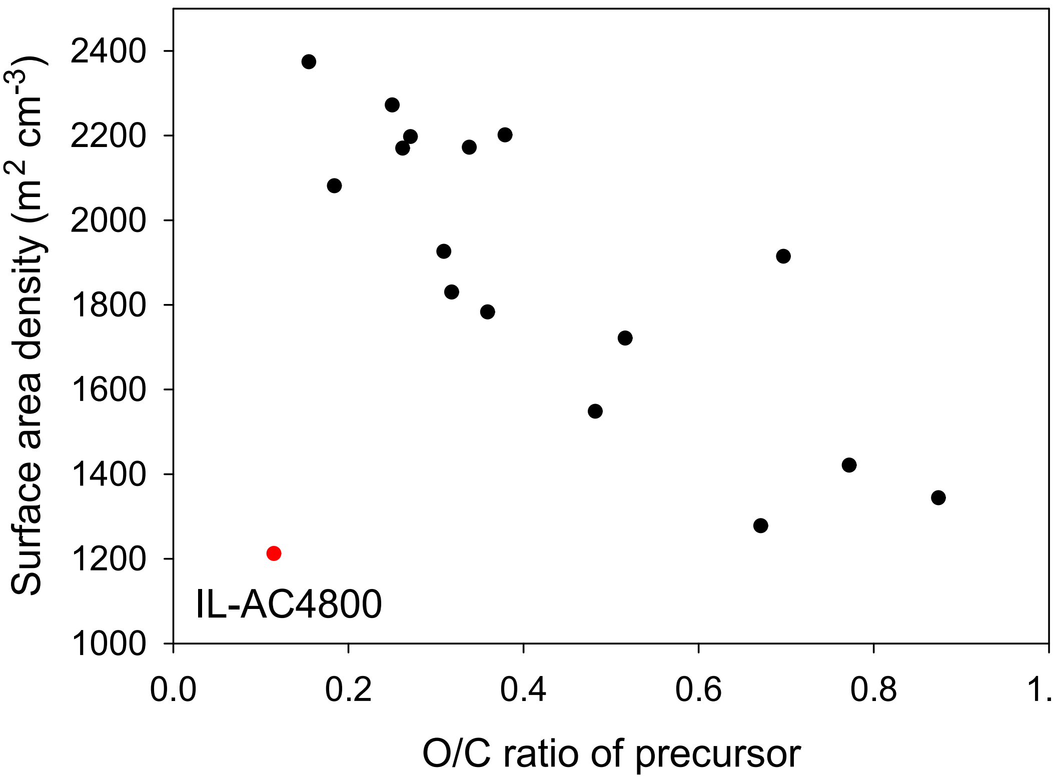

Supplementary Fig. 26 Surface area density of activated carbons as a function of the O/C ratio of the precursor carbonaceous matter. All activations were performed at 800 °C at KOH/precursor ratio of 4.

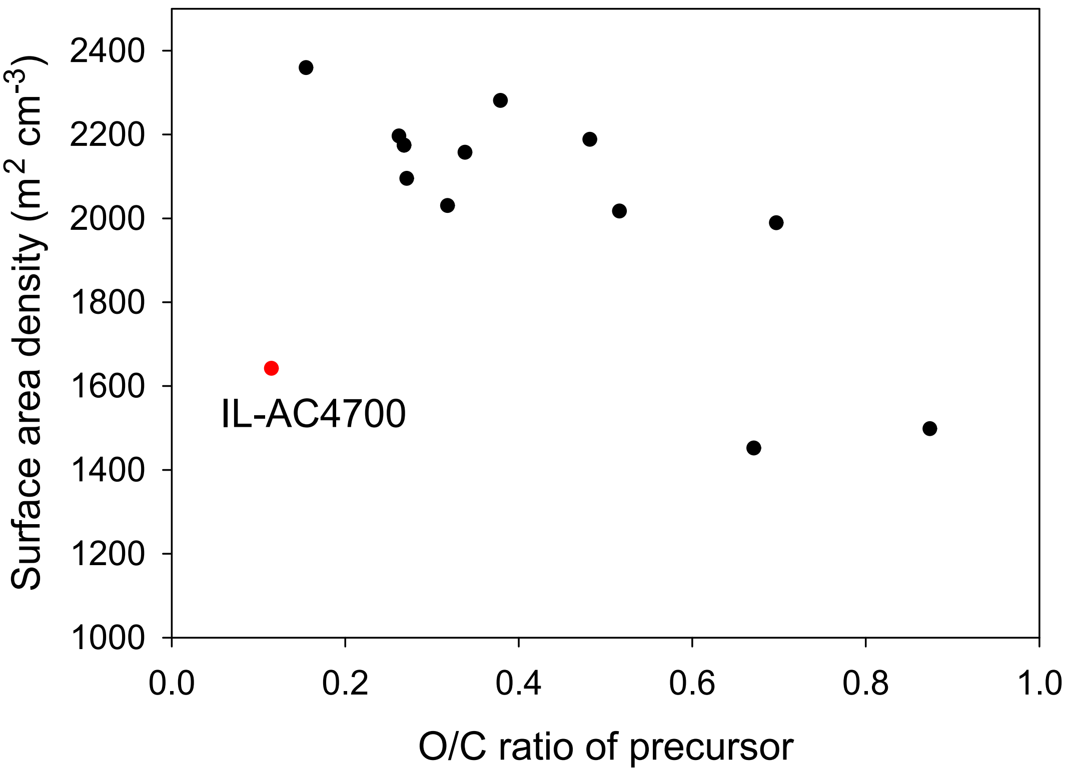

Supplementary Fig. 27 Surface area density of activated carbons as a function of the O/C ratio of the precursor carbonaceous matter. All activations were performed at 700 °C at KOH/precursor ratio of 4.

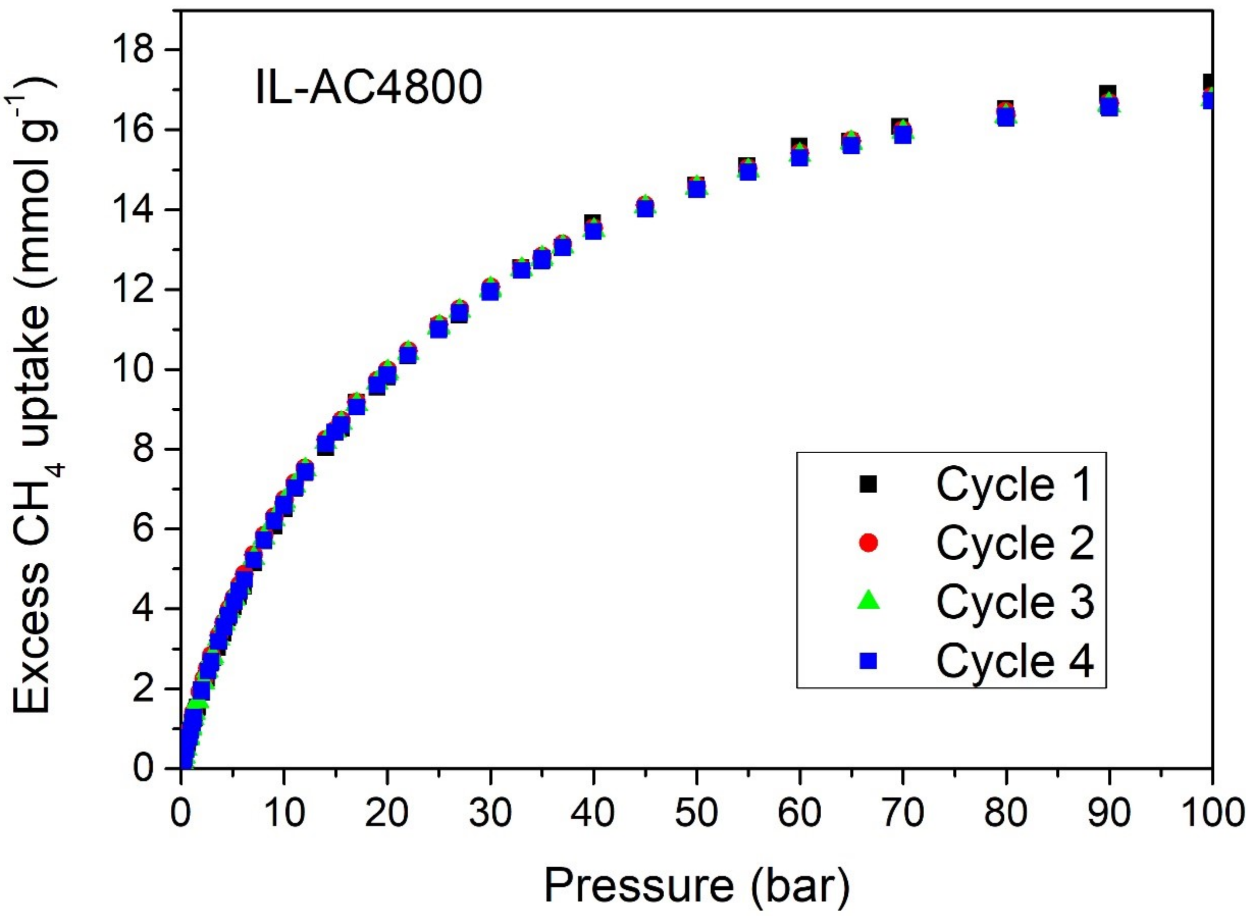

Supplementary Fig. 28 Cyclability of methane uptake and effect of compaction for sample IL-AC4800. Cycle 1 was measured for powdered IL-AC4800, i.e., before compaction, while cycle 2, 3 and 4 were measured after compaction at 370 MPa for 10 min in a 1.3 cm (diameter) die. The data shows a high level of recyclability, and furthermore that compaction has no impact of the methane uptake.

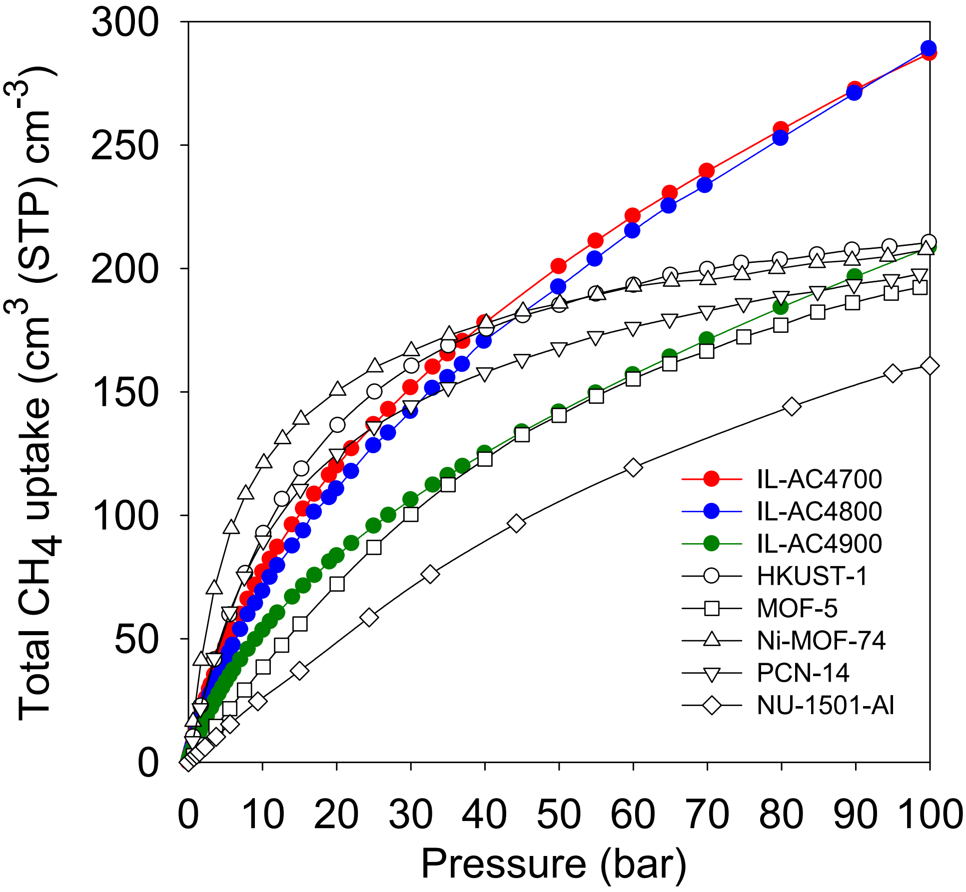

Supplementary Fig. 29 Total volumetric methane uptake at 25 °C of the best performing IL-AC carbons compared to benchmark MOF materials. The uptake of powder MOFs was calculated using crystallographic density and a reduction of 25% was applied to simulate more realistic packing density.

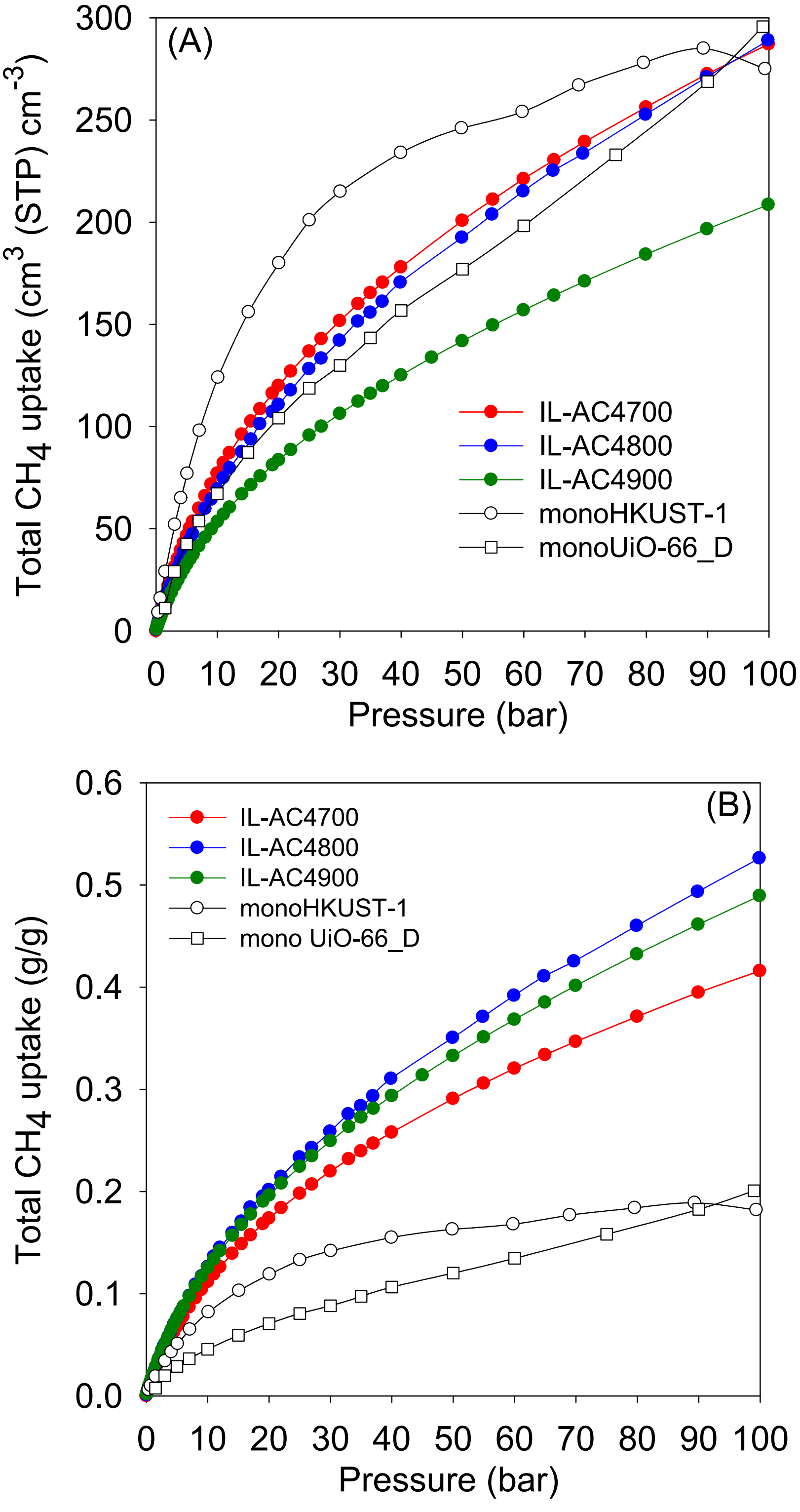

Supplementary Fig. 30 Total volumetric (A) and gravimetric (B) methane uptake at 25 °C of the best performing IL-AC carbons compared to monolithic MOF materials.

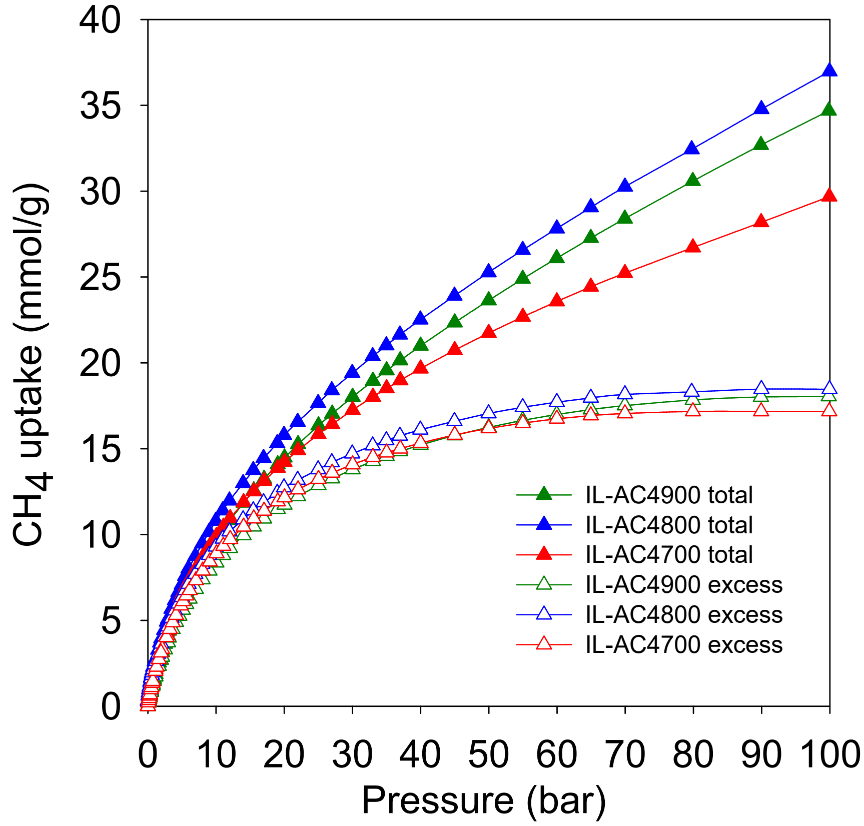

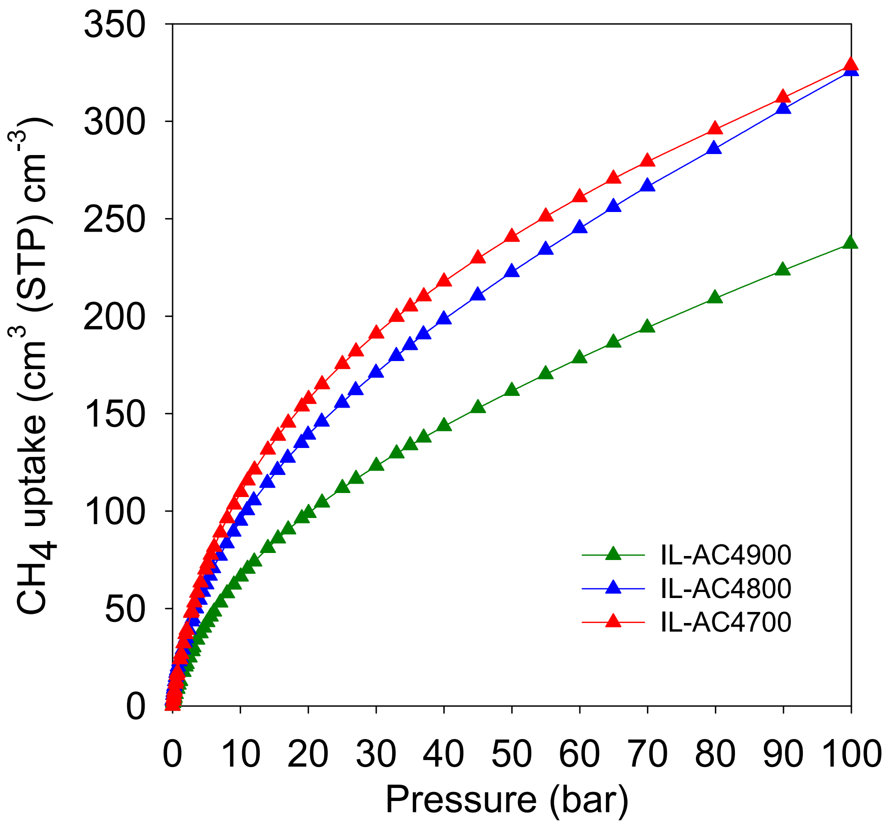

Supplementary Fig. 31 Excess and total gravimetric methane uptake (top) and total volumetric uptake (bottom) for IL-AC4T activated carbons at 0 °C.

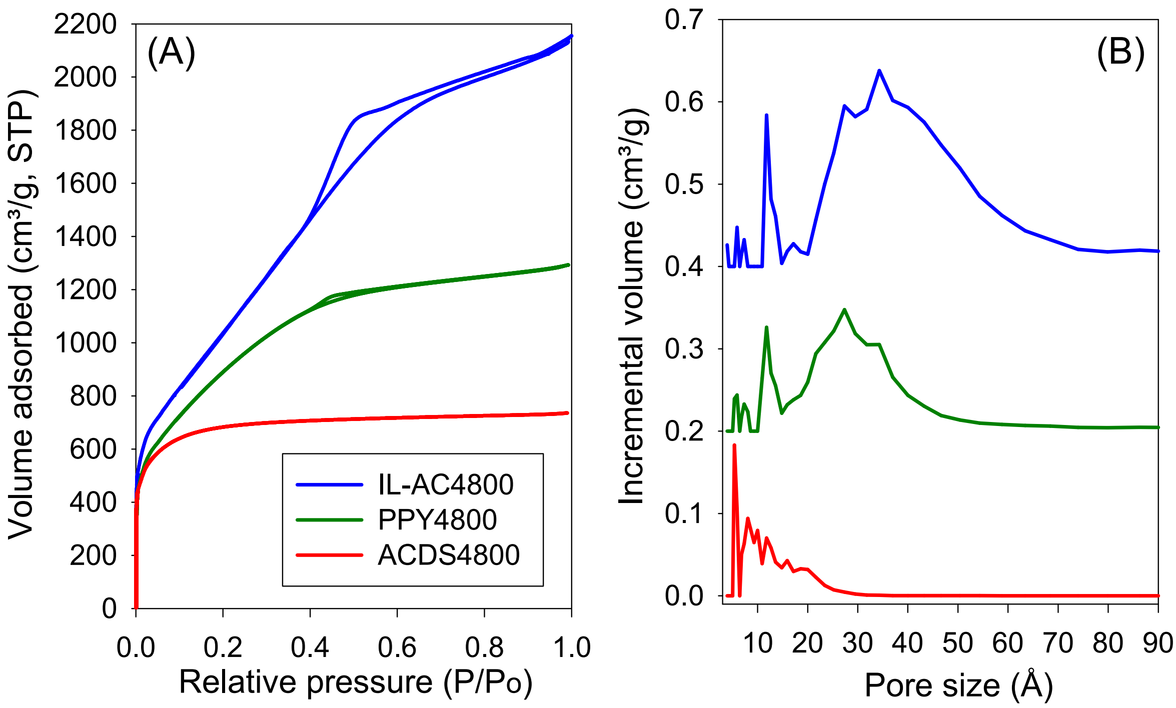

Supplementary Fig. 32 Nitrogen sorption isotherms (A) and correponsing pore size distribution cirves (B) of IL-AC4800 compared to similarly activated carbons prepared from other precursors; ACDS4800 from air-carbonised date seed (ACDS) and PPY4800 from polypyrrole (PPY).

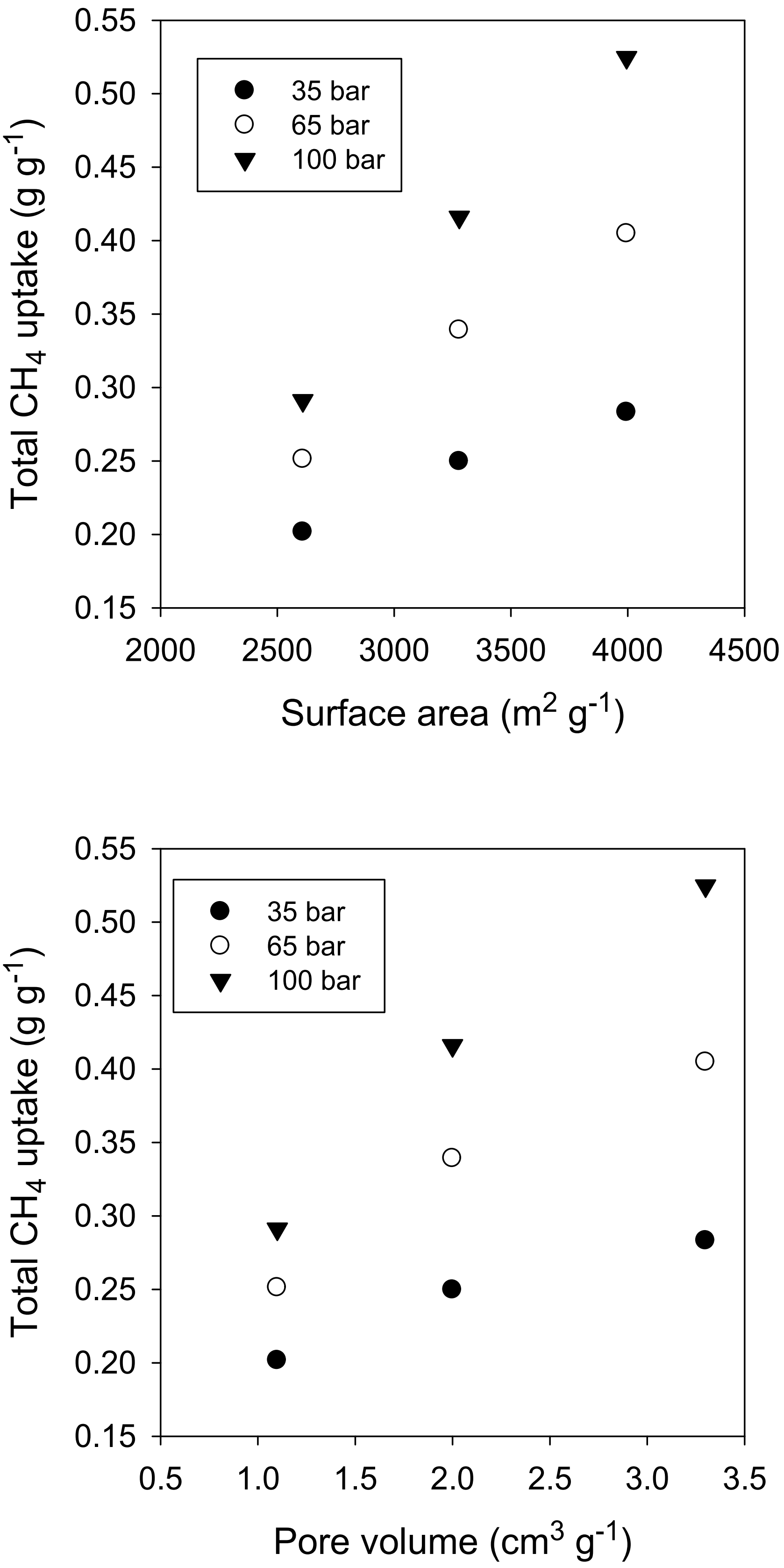

Supplementary Fig. 33 Total gravimetric methane storage capacity of IL-AC4800, ACDS4800 and PPY4800 carbons at 25 ^{o}C and various uptake pressures plotted as a function of surface area (top) or pore volume (Bottom).